



## Quantifying wetland microtopography with terrestrial laser scanning

Atticus E.L. Stovall<sup>a,b,\*</sup>, Jacob S. Diamond<sup>c</sup>, Robert A. Slesak<sup>d</sup>, Daniel L. McLaughlin<sup>c</sup>, Hank Shugart<sup>b</sup>



<sup>a</sup> NASA Goddard Space Flight Center, Greenbelt, MD, USA

<sup>b</sup> Department of Environmental Sciences, University of Virginia, Charlottesville, VA, USA

<sup>c</sup> Department of Forest Resources and Environmental Conservation, Virginia Polytechnic Institute and State University, VA, USA

<sup>d</sup> Minnesota Forest Resources Council, St. Paul, MN 55108, USA

### ARTICLE INFO

Edited by: Emilio Chuvieco

Keywords:

3D  
Hummock  
Hollow  
Hydrology  
Terrestrial LiDAR  
Algorithm  
Automatic  
Sensitivity  
Model resolution  
Classification  
Machine learning

### ABSTRACT

Wetlands hold the highest density of belowground carbon stocks on earth, provide myriad biogeochemical and habitat functions, and are at increasing risk of degradation due to climate and land use change. Microtopographic variation is a common and functionally important feature of wetlands but is challenging to quantify, constraining estimates of the processes and functions (e.g., habitat diversity, carbon storage) that it regulates. We introduce a novel method of quantifying fine-scale microtopographic structure with Terrestrial Laser Scanning using 10 black ash (*Fraxinus nigra*) wetlands in northern Minnesota, USA as test cases. Our method reconstructs surface models with fine detail on the order of 1 cm. Our independent validation verifies the surface models capture hummock (local high points) and hollow (local low points) features with high precision (RMSE = 3.67 cm) and low bias (1.26 cm). A sensitivity analysis of surface model resolution showed a doubling of model error between 1 cm and 50 cm resolutions, suggesting high-resolution reconstructions most precisely capture surface variation. We also compared five classification methods at resolutions ranging from 1 cm to 1 m and determined that maximum likelihood classification at 25 cm resolution most accurately (78.7%) identifies hummock and hollow features, but a simple thresholding of surface model elevation and slope was ideal for hummock feature delineation, retaining over 91% of hummock areas. Finally, we test and validate a novel microtopographic delineation method (TopoSeg) that accurately (Bias = 0.2–11.9%, RMSE = 19.6–24.1%) estimates the height, area, volume, and perimeter of individual hummock features. For the first time, we introduce an accurate and automated approach for quantifying fine-scale microtopography through high resolution surface models, feature classification, and feature delineation, enabling geospatial statistics that can explain spatial heterogeneity of habitat structure, soil processes, and carbon storage in wetland systems.

### 1. Introduction

Wetlands provide important biological (Semlitsch and Bodie, 2003), biogeochemical (Capps et al., 2014), and hydrological functions (Acreman and Holden, 2013), all largely driven by wetland soil profiles and surface topography (Ehrenfeld, 1995; Stribling et al., 2006). Microtopography, or the small scale ( $10^{-1}$ – $10^0$  m) variation in ground surface elevation, is a commonly observed, but rarely measured, feature of wetlands. Small microtopographic changes often have major implications, creating spatial heterogeneity in biogeochemical and habitat conditions. Even slightly elevated areas can have reduced soil moisture and thus increased oxygen availability, with important implications for soil nutrient cycles (Courtwright and Findlay, 2011), plant regeneration and productivity (Watts et al., 2010), and carbon processing (Bubier

et al., 1995). Thus, quantifying fine-scale variation in wetland surface elevation is important to understand drivers and variability of many wetland functions, particularly their critical role in global carbon budgets (Sullivan et al., 2008).

The structure and spatial pattern of microtopographic wetland features vary widely across systems and are inherently challenging to quantify with fine-scale resolution. Wetland microtopography is often typified by local high points ("hummocks") interspersed among more abundant low points ("hollows"). Despite the importance of microtopography on wetland structure and function, methods to quantify it are still rudimentary. Many studies use manual surveys or transects combined with high precision GPS or other survey-grade instruments (e.g. TotalStation), at relatively coarse (1 m) intervals (Ehrenfeld, 1995; Lorente et al., 2012; Pouliot et al., 2011), but transects are unable to

\* Corresponding author at: NASA Goddard Space Flight Center, Greenbelt, MD, USA.

E-mail address: [atticus.e.stovall@nasa.gov](mailto:atticus.e.stovall@nasa.gov) (A.E.L. Stovall).

effectively represent or compare differences in spatial microtopographic patterns (Moser et al., 2007). Further, most studies on microtopography make no attempt to measure fine-scale microtopographic variation itself, instead, relying on categorical analysis of differences between predetermined or field-defined microtopographic groupings (e.g., hummocks versus hollows).

Remote sensing provides more objective and fine-scale measurement of wetlands, enabling better characterization of microtopography. Unoccupied aerial vehicles (UAVs) and structure from motion (SFM) are promising for mapping wetland features (Kalacska et al., 2017), but can only be effectively used in vegetation-free environments. Airborne light detection and ranging (LiDAR) can characterize microtopography, but surface point density and geo-positioning errors reduce the potential resolution and precision of surface models, especially in forested systems. As a result, most studies using LiDAR to quantify wetland features produce surface models of relatively low resolution (e.g., ~1–2 m; Richardson et al., 2010). Some recent studies obtained higher resolution surface models (e.g., ~0.5 m; Baltensweiler et al., 2017; Hopkinson et al., 2005; Knight et al., 2009; Lovitt et al., 2017; Miroslaw-Swiatek et al., 2016), but many microtopographic features are often 0.10–0.30 m in diameter and height (Peterson and Baldwin, 2004; Anderson and Lockaby, 2007; Stribling et al., 2006). This mismatch in scales of microtopography and surface model resolution suggests the need for more fine-scale three-dimensional surface modeling.

Terrestrial laser scanning (TLS) is stationary ground-based LiDAR that produces orders of magnitude higher point cloud density than airborne instruments over smaller areas and provides the necessary detail for capturing fine-scale microtopography. The recent advances of TLS methodology and processing approaches in forest ecology (Atkins et al., 2018; Liang et al., 2016; Stovall et al., 2018, 2017; Stovall and Shugart, 2018), hydrology (Hohenthal et al., 2011), and geomorphology (Stenberg et al., 2016) suggest the potential for new applications and analyses in complex microtopographic systems. While the stationary nature and shallow view angle of TLS presents challenges in sufficient surface coverage—especially in high density understory and ground vegetation (Anderson et al., 2010)—no other technique can resolve fine-scale structure with such detail and with rapid field application.

Despite the advantages of TLS, few studies have used it to quantify microtopographic structure (but see Anderson et al., 2010; Baltensweiler et al., 2017; Rodríguez-Caballero et al., 2016; Stenberg et al., 2016). Of those, no single work has offered a sufficient sampling strategy for larger areas, incorporated a consistent validation method, or assessed the impact of model resolution on quantifying microtopographic variation in wetland systems. In addition, studies lacking vegetation cover (e.g., Stenberg et al., 2016) are not representative of many wetland systems, where dense understory or grasses are common and limit the number of LiDAR returns reaching the ground surface. Last, insufficient TLS sampling (Anderson et al., 2010; Stenberg et al., 2016) typically limits modeling accuracy, and the spatial extent of most studies is less than ~80 m<sup>2</sup> (Anderson et al., 2010; Rodríguez-Caballero et al., 2016; Stenberg et al., 2016), reducing areas of inference and upscaling capacity. One study extensively validated surface models across a large 2 ha mountainous area, but the finest surface model resolution (20 cm) may still be too coarse for many wetland applications (Baltensweiler et al., 2017). Consequently, we suggest that TLS methods in wetland systems must be improved and standardized to ensure unbiased and precise quantification of microtopography.

Limitations of past studies highlight the need for refined TLS methodologies. These should be developed through studies across a range of wetland environments with a consistent sampling strategy, extensive independent validation that can be conducted at the time of TLS sampling, and a fine-scale sensitivity analysis of model resolution. High-resolution microtopographic surface models can potentially provide objective wetland classification, but there is a paucity of reliable, high-resolution surface modeling techniques specific to the challenges

in wetland systems (e.g., ponded water and dense vegetation). Further, higher level three-dimensional analyses of fine-scale microtopography are non-existent in the literature. Specifically, the development of a methodology for rapid and accurate segmentation of individual microtopographic features (i.e., hummocks and hollows) would improve our understanding of their size and spatial distributions, providing greater insights into their role in wetland function (cf. Casey et al., 2016).

Our objectives were: 1) assess the precision and accuracy of high resolution surface models created using refined TLS field sampling, specifically for capturing microtopographic structures in wetlands, 2) determine the impact of model resolution on microtopographic model reconstruction, 3) assess hummock classification accuracy at a range of resolutions using common landform classification methods, and 4) develop and assess a novel method, we call TopoSeg, for delineating individual microtopographic structures (e.g. hummocks) and quantifying their geometric properties. These objectives provide the structural sub-headings used in the Methods, Results and Discussions sections. We believe that establishing a standard methodology for TLS microtopographic data collection and processing will encourage its use in wetland systems across the globe, enabling comparative analysis and addressing system-specific questions.

## 2. Study site

We investigated ten black ash (*Fraxinus nigra* Marshall) wetlands in northern Minnesota, U.S.A (Fig. 1). Using hydrogeomorphology, we characterized each wetland into 3 classes: 1) depression sites ("D", n = 4) characterized by convex, pool-type geometry surrounded by uplands, 2) transition sites ("T", n = 3) characterized as flat, linear boundaries between uplands and black spruce (*Picea mariana* [Mill.] B.S.P.) bogs, and 3) lowland sites ("L", n = 3) characterized by a flat, gently sloping topography. Within each group, wetlands exhibited similar water level dynamics (Table 1) and soils, which were typically deep mucky peats underlain by silty clay mineral horizons. Within each site, we established three clustered 300 m<sup>2</sup> sampling circular plots (~9.8 m radius) located around a randomly established point at each site (Fig. 2).

## 3. Methods

### 3.1.1. TLS acquisition

To ensure high-quality TLS acquisitions, we planned our TLS campaign to coincide with the time of least vegetative cover and the least likelihood for aboveground water. We scanned sites from October 20–24, 2017, averaging two to three sites per day (Table 1). During scanning, leaves from all deciduous canopy trees were off, grasses had largely senesced, and standing water was present at portions of three of the sites (D1, D2, and D3). Where standing water was present, it was typically < 10 cm deep and constrained to small pools (ca. 0.5–2 m<sup>2</sup>) dispersed across the site (Table 1).

To capture high-resolution surface topography, we deployed a Faro Focus 120 3D phase-shift TLS (905 nm  $\lambda$ ) in each of the three clustered plots at each wetland site (Table 1). This phase-shift laser scanner has several notable limitations and benefits relevant to microtopographic surface modeling in wetland systems. The 905 nm wavelength coincides with a range of wavelengths with high water absorption, potentially reducing return intensity at the surface of wet soil, or completely eliminating returns in inundated locations. Other laser scanners, particularly those in the green spectrum (e.g. 532 nm) would be more appropriate choices for wetlands with significant inundation. The single-return nature of the Faro Focus 120 3D should also be considered, as returns are limited at the deepest layers of understory vegetation and grasses. Conversely, the high resolution and low beam

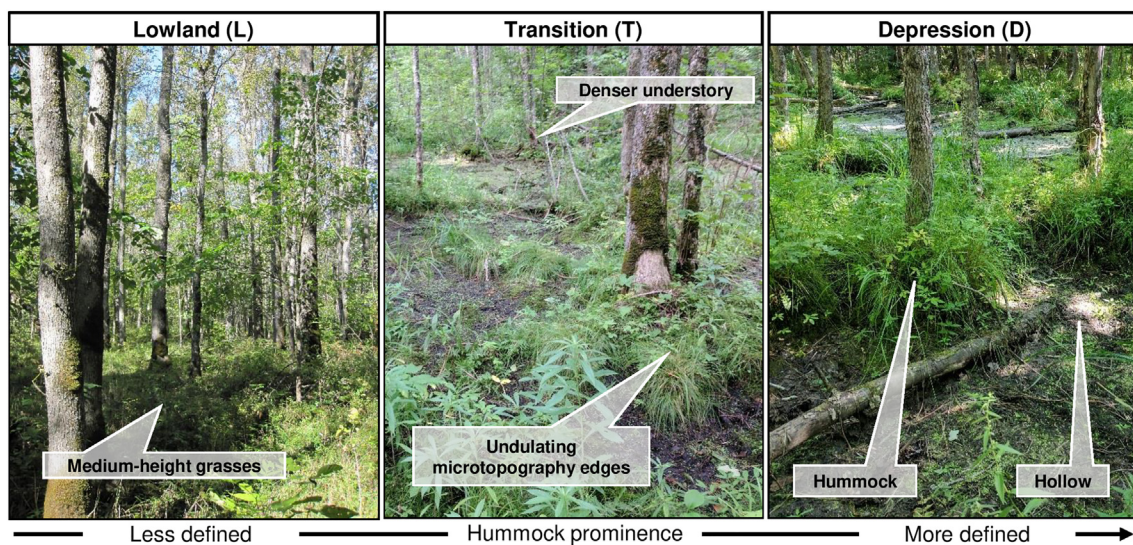


**Fig. 1.** Illustration of microtopography and vegetation typical of site types: lowland (L3), transition (T2), and depression (D2) sites. Lowland sites had the least pronounced microtopography, whereas transition sites and depression sites had more obvious hummock edges and greater elevation differences between hummocks and hollows. Transition sites typically had more complex, undulating hummock features, whereas depression sites exhibited more circular hummock features. Transition sites also had considerably denser understory (i.e., shrubs) than depression or lowland sites, although lowland sites also had a dense grass understory.

divergence mitigate issues of occlusion in dense understory. Though noise in the LiDAR data of phase-shift instruments is often an issue in natural environments, appropriate filtering algorithms improve the resulting point clouds. Finally, phase-shift laser scanners are also significantly lighter in weight, have fast scan times, and are notably less expensive than other time-of-flight sensors with similar specifications.

We strategically planned our LiDAR acquisitions so all three plot-level scans could be merged for a single ~900 m<sup>2</sup> site-level LiDAR dataset. Depending on the density and complexity of understory vegetation, we used one of two configurations for plot-level scans to minimize occlusion of the ground surface (Fig. 2). In open-understory depression sites, the TLS was placed at the plot center and four surrounding locations approximating the cardinal directions, with the distances (approximately 10 m) from the center point dictated by the wetland shape and size (Fig. 2A). In this configuration we scanned at higher resolution (28.2 million pulses per scan) to compensate for reduced scan locations. In mid-density sites (e.g., transition and lowland sites) we opted for increased scan positions at lower resolution (approximately 10 million pulses per scan) placed in a ten meter-spaced grid network within each plot to reduce occlusion of the ground surface (Fig. 2B). With the second scan configuration, we collected an average of nine scans per plot and approximately 300 million pulses per site. In total, 197 scans

were collected across 30 plots and 10 study sites.

To facilitate scan registration, we placed ten 7.62 cm radius spheres for maximum visibility in each plot. Once scans within a plot were completed, all registration spheres, except 2–3 immediately adjacent to the subsequent plot, were relocated to the next plot location. The remaining, unmoved, spheres were included in the initial scans of the subsequent plot to facilitate site-level registration. Immediately after the initial three scans on the second plot, the registration points used to register the plots together were moved, to link to the next plot of interest. This approach and the close plot clustering within a site facilitated registration across the three plots, ultimately allowing site-level TLS data for large area surface models.

### 3.1.2. Field protocol for TLS surface model validation

To validate the TLS surface model products, we installed twenty 2.54 cm radius spheres on 1.40 m fiberglass stakes such that the spheres were exactly 1.20 m above ground surface (Fig. 2C; D). We placed validation spheres approximately plumb to reduce errors due to horizontal misalignment. We located the validation points directly in the TLS data to assess the precision and accuracy of the final surface models; we subtracted 1.20 m from each located validation point to get the true height of the soil surface. While this method of surface model

**Table 1**

Summary of site information, TLS registration statistics, and acquisition parameters.

Site	Latitude	Longitude	Elevation (m)	Size (ha)	Sample date	Registration statistics (m)			Scan metadata				Water table (m)		
						Mean	SD	Max	Positions	Pattern	Resolution (mrad)	Pulses (Mpts)	Water	Mean	SD
L1	47.100	-92.545	403	2.191	22-Oct-2017	0.004	0.0048	0.0338	24	Dense	0.070	657	-	-0.255	0.462
L2	46.916	-93.359	391	6.845	22-Oct-2017	0.0033	0.004	0.0226	23	Dense	0.070	630	-	-0.346	0.543
L3	47.078	-91.774	394	1.455	22-Oct-2017	0.0041	0.0083	0.0619	24	Dense	0.070	657	-	-0.370	0.502
D1	47.672	-93.684	447	5.697	23-Oct-2017	0.0027	0.0039	0.0209	18	Open	0.044	784	+	0.012	0.179
D2	47.281	-94.384	425	6.499	20-Oct-2017	0.0067	0.0047	0.0524	13	Open	0.044	566	+	-0.007	0.156
D3	47.284	-94.380	429	6.062	20-Oct-2017	0.0036	0.0038	0.0155	12	Open	0.044	523	+	0.053	0.196
D4	47.280	-94.486	442	0.491	21-Oct-2017	0.0041	0.0039	0.0159	12	Open	0.044	523	-	-0.008	0.151
T1	47.837	-93.713	424	15.659	23-Oct-2017	0.0011	0.0024	0.0146	21	Dense	0.070	575	-	-0.001	0.125
T2	47.679	-93.915	447	8.618	23-Oct-2017	0.0049	0.0059	0.033	19	Dense	0.070	520	-	-0.048	0.202
T3	47.276	-94.487	432	1.938	21-Oct-2017	0.0029	0.0034	0.0142	23	Dense	0.070	630	-	-0.069	0.217

+ Standing water present or site partially inundated.

- Standing water absent from site.

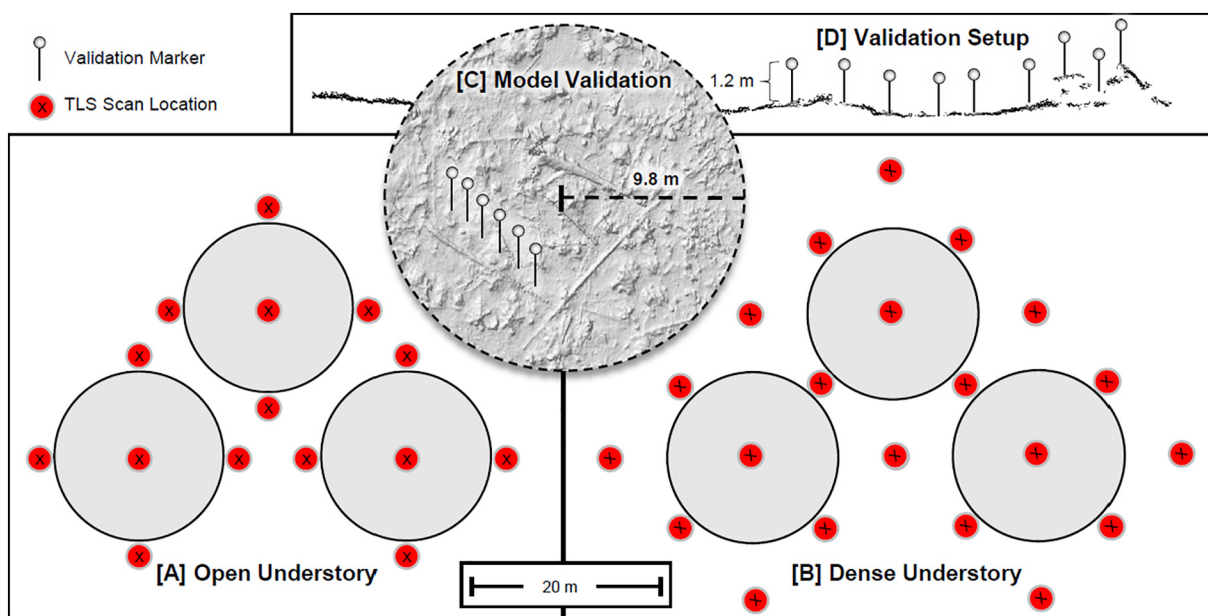


**Fig. 2.** Scan configuration in (A) open and (B) dense understory, with red "X" symbols indicating scan locations. The three clustered 9.8 m radius plots for each site are shown in grey. The open understory configuration emphasized precise, high resolution surface models, and the dense understory configuration was optimized to minimize hummock and hollow occlusion in the final model. (C) We assessed model precision and accuracy with 20 validation points placed 1.2 m aboveground (hillshaded surface model shown in background). (D) We located the validation points in the TLS scans and subtracted 1.2 m from the validation point height to estimate the height of the true ground surface. The transect shows a 10 m long by 10 cm wide area extracted from the identified TLS ground returns. (For interpretation of the references to colour in this figure legend, the reader is referred to the web version of this article.)

validation used the same instrumentation for model creation and validation, we did not rely on the validation points for model creation, making the two datasets independent. An added benefit of this method is that the ranging error for the TLS was on the order of 5 mm, significantly less than the location error typical of precision GPS units, though slightly higher than a total station. Moreover, since our method does not rely on the number of available GPS satellites, it was less influenced by dense canopy cover and understory vegetation, making it more suitable for assessing fine-scale topographic variation in a range of site conditions. Lastly, this approach avoided the need for additional instrumentation in remote field locations, allowing model validation at the time of the TLS acquisition.

### 3.2. Model development

In the following four sections, we describe the stages of a processing pipeline used to create high-resolution surface models from raw TLS point cloud data and create segmented hummock features for deriving geometric properties, such as height, area, perimeter-area ratio, and volume (Fig. 3). In Stage 1, the raw TLS scan data are merged, processed, and filtered. Stage 2 removes overlying vegetation from the merged TLS data and produces the initial microtopographic surface model. Stage 3 detrends site-wide topography and classifies potential hummock areas. Finally, Stage 4 uses a modified watershed delineation approach (TopoSeg) to detect and segment individual hummock features. Sensitivity analyses and error assessment of the surface models and the TopoSeg algorithm, including an analysis of more sophisticated classification algorithms are detailed in Section 3.3.

#### 3.2.1. Stage 1: post processing

We registered and filtered TLS scans using the algorithms included in Faro SCENE (SCENE (version 5.4.4.41689), 2015). Registration for each plot relied on digital recognition of registration spheres ( $n = 10$ ; see Section 3.1.1). All visible spheres were digitally located in each scan and aligned with corresponding spheres in other scans from that plot. Plot-level registration error was quantified as the least squares fit of

corresponding sphere objects in SCENE (mean = 3.77 mm,  $sd = 4.85$  mm). High precision in the registration stage – below the target resolution of the final surface model – is essential for quality surface models. We reduced noisy LiDAR returns for object edges and points close to the TLS range limit with intensity and stray point filters (Fig. 3, Stage 1) following Stovall et al. (2017). Specifically, the intensity filter removes “dark returns” (< 650 intensity; maximum intensity = 2100), the threshold of which was chosen to ensure distant low intensity returns were excluded, but high-moisture soil returns were retained. We also implemented a stray point filter to eliminate ambiguous ranging errors via a moving  $3 \times 3$  grid cell window with a 20% retention and 1 m distance threshold (Stovall et al., 2017). We exported the filtered point cloud data in XYZ (ASCII) format for further processing.

#### 3.2.2. Stage 2: microtopographic surface model generation

We created a high-resolution (1 cm) surface model for each site from the registered and filtered point cloud data using a series of steps (Fig. 3, Stage 2) and the command line mode of CloudCompare software (Othmani et al., 2011). We first clipped the point cloud to 1 m above and below the approximate ground surface to reduce computation time. We then used two iterations of a statistical outlier removal filter to remove spurious and noisy scan points that would distort the final surface model (Rusu and Cousins, 2011). The filtering method, based on the Point Cloud Library (PCL), assumes a Gaussian distribution of nearest neighbor distances. Point distances exceeding a defined threshold of standard deviation from the mean point distance are deemed outliers and are removed. We identified outliers as points exceeding two standard deviations of the mean of 6 nearest neighbors (Stovall et al., 2017).

We rasterized the point cloud with the *rasterize* tool in CloudCompare, using the absolute minima in a moving 5 mm grid (Fig. 4A). The method did not interpolate elevation values in empty raster cells. A triangulated irregular network (TIN) method – creating a three-dimensional surface of the point cloud with interconnected triangles – can be used at this stage for an alternative surface model, but,

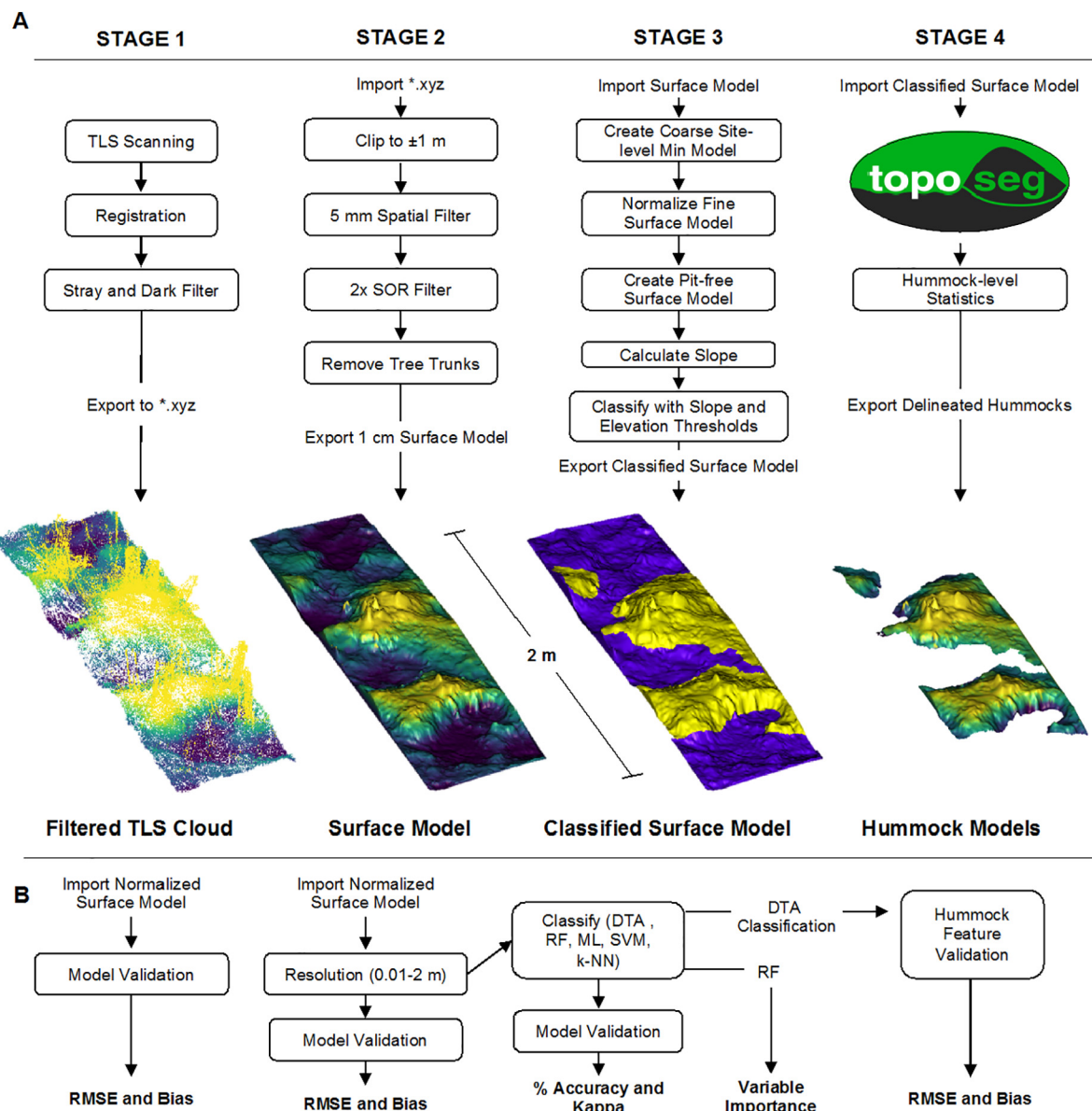


**Fig. 3.** [A] Processing workflow and [B] set of analyses for assessing the microtopographic surface modeling and hummock delineation. In Stage 1, the raw TLS data undergo initial post processing, filtering, and are exported. Stage 2 removes overlying vegetation and creates the 1 cm surface model. Stage 3 normalizes the surface model and identifies area to focus hummock detection. Finally, in Stage 4, local maxima are detected and, with a watershed delineation approach (TopoSeg), hummocks are detected for site-level hummock statistics. [B] The set of analyses were selected to assess the effects of model resolution (1 cm to 2 m), classification method (Digital Terrain Analysis (DTA) Threshold, Random Forest (RF), Maximum Likelihood (ML), Support Vector Machines (SVM), and k-Nearest Neighbor (k-NN)), and variable selection (based on Random Forest variable importance), as well as quantitatively validate the hummock feature delineation algorithm. The surface modeling workflow and TopoSeg are freely available at <https://github.com/aestovall/TopoSeg>.

based on previous high-resolution TLS surface modeling (Baltensweiler et al., 2017), we anticipated little difference in modeling approaches at this high-resolution stage.

A slope analysis approach was used to remove points associated with tree trunks, often co-located with hummocks (Fig. 4B). We implemented the *gradient* tool in CloudCompare to calculate the slope of the 5 mm surface model, and then used slope steepness to identify and remove extraneous points. Through visual interpretation of several plots, we determined a grid-cell slope value of 40% to be an appropriate upper bound threshold to filter extraneous points from understory vegetation and most overlying trunk points. The slope threshold is a user variable parameter and can be adjusted according to site conditions.

After removal of trunk and understory points, we implemented an additional outlier removal filter following the same method as described above (removing points with distances greater than two

standard deviations of the 6 nearest neighbors) to ensure all points above ground level were excluded. We meshed the remaining slope-filtered point cloud using the same local minima approach described above at 1 cm resolution (Fig. 4). The resulting final surface model effectively represented the ground surface and was less influenced by overlying vegetation (Fig. 4). We implemented the CloudCompare processing within an R (R Core Team, 2017) processing framework to automate and streamline site-level processing.

### 3.2.3. Stage 3: classifying hummocks versus hollows

After we created 1 cm surface models of each site, we classified the surface model into two elevation categories: hummocks and hollows (Fig. 3, Stage 3). We first detrended site-scale elevation gradients (typically on the order of 10 cm) that would confound our elevation-based classification scheme. To do this, we used a standard airborne LiDAR

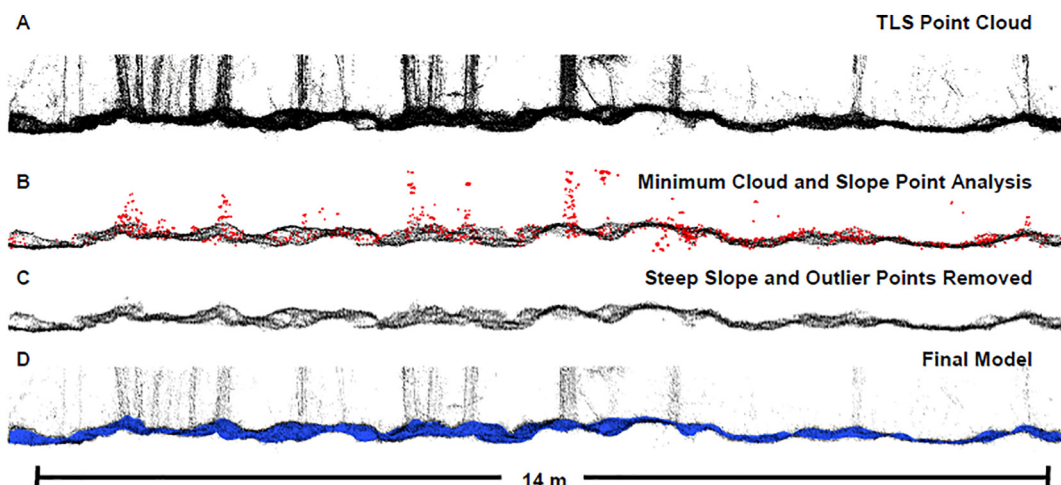


**Fig. 4.** Transect showing the TLS point cloud and final surface model at all major processing stages (site T1 shown). (A) We start with the raw TLS point cloud and remove overlying vegetation points using slope and outlier removal. (B) The 5 mm minimum TLS point cloud is filtered by identifying points with a local slope estimate of 40% (red). (C) The steep slope points are removed and point cloud outliers are removed, resulting in a clean point cloud for high resolution surface reconstruction. (D) The final 1 cm surface model (blue) clearly reconstructs hummock and hollow features, without being impacted by dense vegetation (black). See Fig. S1 (Supplementary Material) for oblique view of the above transect. (For interpretation of the references to color in this figure legend, the reader is referred to the web version of this article.)

processing approach of topographic detrending implemented in *CloudCompare* (2018) with the *cloud to mesh distance* tool. We first created a coarse – 2 m resolution – Digital Earth Model (DEM) from the lowest points of the 1 cm resolution model. The coarse 2 m model was created using a TIN approach. The method effectively removed broad, site-level topography and resulted in less artifacts in the normalized high-resolution surface models. We then detrended the site-wide elevation gradient by subtracting the 2 m site-wide DEM from the 1 cm surface model. The normalized, or detrended surface model, was used for all future processing, including the classification sensitivity analysis described in Section 3.3.3.

We converted the normalized surface model into a gridded set of points and created a “pit-free” surface model using the pit-free grid canopy function (Khosravipour et al., 2014) in the R package, *lidR* (Roussel and Auty, 2018). This pit-free surface model fills gaps in the original surface model with small disks that buffer at a specified distance (4 cm, for this study) around the points in the surface model. The resulting rasterized surface models had less gaps and were better suited for continuous wetland classification.

We classified the surface models using a combination of normalized elevation and slope thresholds. To ensure our classification was as conservative as possible in identifying potential hummock areas, we relied on a simple digital terrain analysis (DTA) thresholding approach common in large-scale ALS-based wetland area detection (Richardson et al., 2009). We used a DTA threshold classification approach to identify areas with both low elevation and low slope as hollows. To avoid confounding hollows with the tops of hummocks (tops of hummocks are typically flat or shallow sloped), we limited our classification of hollows to the lower 50% elevations of the surface model. In order to make the thresholds adaptive to individual site characteristics, we set both slope and elevation thresholds as the 50th percentile of values at each site. The ultimate goal of this simple classification was to conservatively limit the area included in subsequent hummock delineation, however we also tested more sophisticated feature classification methods, described in Section 3.3.3. After hollow classification, we used the remaining surface model area as our domain of potential hummocks.

#### 3.2.4. Stage 4: TopoSeg hummock delineation

To enable analyses of individual hummock structures and patterning, we developed a hummock segmentation routine – TopoSeg –

that segments hummocks into individual objects and enables the measurement of a range of geometric properties (Fig. 3, Stage 4). We first used the local maxima (Roussel and Auty, 2018) of a moving window to identify potential microtopographic structures for segmentation. We chose a  $21 \times 21$  cm window for the local maxima estimation as this size was representative of observed hummock dimensions and was approximately less than the average spacing between observed hummock maxima. The size of the window is a parameter that can be varied according to the model resolution and characteristic size of the microtopography. A height threshold defines the area above which local hummock maxima can be identified.

The local maximum serves as the “seed point” from which we apply a modified watershed delineation approach (Pau et al., 2010). The watershed delineation functions as an inverse watershed function, inverting the elevation values in the surface model and finding the edge of the “watershed”, which in this case are hummock edges. The defined boundary clips and segments an identified hummock area into a single surface model. Watershed delineation is novel in microtopographic analysis and it can potentially provide additional information on individual hummock geometry, beyond simple binary classification. We note, watershed delineation is also capable of effectively classifying hummock and hollow areas, but more importantly it allows the segmentation of individual hummock features, allowing both site-scale and hummock-scale spatial analysis, useful for studies focused on the development and spatial arrangement of microtopographic features.

TopoSeg allowed us to derive hummock-level metrics describing total area, volume, height, and perimeter-area ratio for each of the segmented hummock objects. These metrics are arguably the most important for future assessment of microtopography and associated functions as they control both the sharp redox gradients which drive biogeochemical processing and the complex hydraulics of wetlands (Frei and Fleckenstein, 2014; Frei and Peiffer, 2016). We calculated area as the total number of pixels in each hummock multiplied by the model resolution ( $1 \text{ cm}^2$ ). Volume was calculated using the same method as area, but multiplied by the height above the normalized hollow surface. The method of volume estimation assumes a rasterized surface, but other 3D methods could be implemented, specifically 3D convex hull or TIN approaches, but, with TLS surface modeling at high resolutions, the method of interpolation has been found to be of less influence on surface model error (Baltensweiler et al., 2017). Perimeter was estimated by converting our raster-based hummock features into

**Table 2**  
Summary of parameters used in the current study and the main findings from the analyses conducted.

Test	Sites	Resolution	Classification	Variables	RMSE	Bias	Accuracy	Summary
Model validation	All	0.01 m	–	DEM, Slope	0.024–0.058 m	0–0.033 m	–	D and T sites had low RMSE and bias. L sites, higher due to surface occlusion.
Resolution sensitivity	All	0.01–2 m	–	DEM, Slope	0.025–0.13 m	–0.01–0.07 m	–	1 cm resolution best for microtopographic surface reconstruction.
Dem dependent error	All	0.1 m	–	DEM, Slope	–	–	–	Surface model error increases with decreasing LiDAR return density at surface.
Classification sensitivity	D2	0.01–1 m	DTA Threshold, RF, ML, SVM, k-NN	DEM, Slope, Roughness, TRI, Intensity	–	–	39–70%	25 cm resolution is best. Maximum likelihood performed best. SVM performed worst. DTA threshold conservatively retains hummocks.
Predictor importance sensitivity	D2	0.01–1 m	RF	DEM, Slope, Roughness, TRI, Intensity	–	–	62%	25 cm resolution is best. DEM is consistently best predictor for all resolutions. Roughness, TRI, and slope important at best resolution.
Hummock delineation distribution KS test	D2, T1	0.01 m <sup>a</sup>	DTA Threshold	DEM, Slope	–	–	$p \geq 0.45$	KS test shows automatic delineation equivalent to manually delineated hummock size distributions.
Hummock Delineation Validation 1:1 Test	D2, T1	0.01 m <sup>a</sup>	DTA Threshold	DEM, Slope	19.6–24.1%	–11.9–0.2%	–	1:1 comparison shows automatic delineation accurately segments hummock features with a slight negative bias compared to manual.

<sup>a</sup> Hummock delineation relies on a 4 cm resolution DEM for the DTA threshold classification. Final surface models are derived from the 1 cm DEM for the most accurate surface reconstruction.

polygons and extracting the edge length from each hummock. The perimeter area ratio represents an approximation of hummock edge complexity (Sheffer et al., 2013) – a higher perimeter:area implies hummocks with increasingly complex edges. Understanding hummock perimeter:area distributions may provide additional insights into the scaling of biogeochemical processes within and among wetlands (cf. Cohen et al., 2016).

### 3.3. Model assessment

To assess precision and accuracy of our microtopographic models, we validated all site-level surface models using 600 independent surface elevation estimates derived from the 2.54 cm spheres described in Section 3.1.2. We evaluated the influence of model resolution on RMSE and bias by varying model resolution from 1 cm to 2 m. We conducted a detailed sensitivity analysis of error and bias by varying both model resolution and classification methodology. Finally, at two sites (D2 and T1), we assessed the precision and accuracy of a novel hummock delineation algorithm – TopoSeg – by comparing geometric measurements for automatic and manually segmented hummock features. See Fig. 3B for a visualization of the analyses and Table 2 for a summary of parameters used and analyses conducted to evaluate microtopographic surface model reconstruction, classification, and feature delineation.

#### 3.3.1. Site-level surface model validation

We validated our surface models with known surface elevation measurements and coverage density analysis. We located a maximum of 20 spheres in each scan for model validation (see Section 3.1.1; Fig. 2). Surface validation point height was calculated by subtracting the validation stake height (1.20 m) from the center of the validation sphere z-coordinate associated with a XY location on surface model grid. We then matched the surface model XY coordinates with the validation point location and compared the validation heights to surface model elevations using a point-to-pixel distance calculation. These paired values allowed us to assess RMSE and bias of the surface models. At all validation points, we extracted a LiDAR return density, defined as the number of returns per square meter, at 1 m resolution, to assess the impact of LiDAR return density on model reconstruction errors. We conducted this analysis for each wetland type (D, T, and L sites) and aggregated across all sites, evaluating model error as a function of coverage density. Finally, we applied a mask over low point density areas, reducing uncertainty in the our final surface models.

Though our method of relying on control points placed a known distance aboveground is less common in model validation, we found it ideal in this study for several reasons. Typical approaches for validating higher-resolution surface models, most often in airborne LiDAR applications, require a high-precision GPS unit measuring surface elevation to be directly matched to a LiDAR-derived surface elevation model (Richardson et al., 2010). In most airborne applications, the validation points (i.e., from GPS) are presumably of significantly higher precision and accuracy than the LiDAR returns used to construct the surface model, and thus are appropriately used for independent surface model validation. However, TLS ranging data have a precision and accuracy on the order of millimeters – significantly more precise than most high-precision GPS units. As such, we opted to use validation points (small spheres 1.20 m aboveground) that we manually located within the TLS data, as opposed to relying on a separate GPS unit that would potentially introduce unnecessary geolocation error in the validation data. The major benefits of using the TLS data to locate our control points for validating our surface model include the lack of geolocation errors, positional errors on the order of millimeters, no requirement for transformation between coordinate systems, and by elevating the control points we mitigated occlusion from dense understory vegetation. The approach used here is analogous to similar studies relying on a Total Station and standing targets, but with a TLS in place as the ranging instrument. We anticipate, future studies relying on TLS to capture

microtopography will adopt a similar methodology, as it is an efficient and precise method of evaluating ultra-fine-scale microtopographic models with millimeter precision.

### 3.3.2. Sensitivity analysis of model resolution

To determine the impact of model resolution on surface model precision and accuracy, we performed a sensitivity analysis where we varied model resolution from 1 to 10 cm at 1 cm intervals, 10–100 cm at 10 cm intervals, and 100–200 cm at 25 cm intervals. We report model validation error and bias both on a site (e.g., D1, L1, T1) and site-type (i.e., D, L, or T) basis. We used the results from the sensitivity analysis to select the optimal model resolution based on the lowest RMSE and bias and used this resolution to model all sites.

### 3.3.3. Sensitivity analysis of hummock classification

To evaluate the accuracy of hummock classification, we compared manually and automatically classified surface models at one depression site (D2) with clearly defined hummock features. We also classified hummocks on a portion of site T1, but excluded it from the classification assessment, as site-wide hummock features were complex, reducing our confidence in the manual approach. We omitted using a lowland site for validation because none of these sites had obvious hummock features that we could manually delineate with confidence.

We manually classified hummocks for the D2 site with a qualitative visual analysis of raw TLS scans (Fig. S2, Supplementary Material). Using the clipping tool in CloudCompare (2018), we clipped hummocks from the raw TLS point cloud and labeled them with unique identifiers. We manually delineated hummocks that were visually obvious and prominent, resulting in a subset of the overall number and distribution of hummocks. We also manually clipped large downed woody-debris (i.e., fallen trees) and excluded them from the hummock validation to limit the comparison to what would traditionally be considered “hummocks”. This manual delineation process was primarily based on field experience and knowledge of what constitutes a hummock in these systems. In this way, our manual delineation is analogous to current observational methods of delineating hummocks from hollows, albeit via raw TLS data versus field observation or survey data.

Using our manual classification of hummock and hollow areas, we assessed the impact of variable selection, model resolution, and classification methodology on hummock and hollow classification accuracy. We tested an array of predictive variables for machine learning-based hummock-hollow classification, specifically the TLS surface model, gridded minimum LiDAR return intensity, slope, terrain ruggedness index (TRI), and roughness – all common in LiDAR-based wetland classification (Richardson and Millard, 2018). The predictive variables were matched with the manually classified raster at site D2. We randomly selected 5000 locations from the manually classified hummock and hollow raster as our training set for classification. We trained the classifiers with 10% of the samples and reserved 90% for independent validation. We focused our analysis on common classification methods used in wetland ecosystems with LiDAR datasets including maximum likelihood (Anderson et al., 2010), random forest, support vector machines, and k-nearest neighbor (Korpela et al., 2009), implementing them using the *Rstoolbox* package in R.

We evaluated the simple DTA threshold approach that relied on slope and the DEM (See Section 3.2.3). The DTA threshold approach was primarily used as a conservative and inclusive estimate of hummock areas, since the resulting classification would later be used in the hummock delineation algorithm. Since this classification approach was based on variable thresholds and not predictive in nature, we directly compared the classification with the manually classified hummock and hollow raster on a pixel-to-pixel basis to assess classification accuracy.

We evaluated classification sensitivity to model resolution between 1 cm and 1 m. All lower resolution microtopographic surface models were based on the highest resolution 1 cm and gridded to 5 cm, 10 cm, 25 cm, 50 cm, and 1 m using k-nearest neighbor interpolation with

inverse-distance weighting. To evaluate variable importance at a range of resolutions, we used the unique ability of random forest to determine individual variable importance in the final classification model for each resolution tested. Finally, for every unique combination of resolution and classification method we evaluated hummock classification accuracy and report kappa statistics to evaluate overall classification accuracy.

### 3.3.4. Hummock delineation error assessment

To evaluate the TopoSeg algorithm, we compared the size distribution and individual hummock geometric properties to a manually delineated dataset at one depression site (D2) and one transition site (T1), both with clearly defined hummock features. These two sites were chosen as they had the highest confidence in manual delineation. The validation data was created using the same manual identification approach described in Section 3.3.3, but we instead retained individual hummock features with unique ID numbers for comparison. We directly compared individual hummocks from the TopoSeg approach to the same hummocks obtained from the manual delineation (Fig. S3, Supplementary Material). To assess bias and error of the delineation method, we matched manual and automatically delineated hummocks for a subset of 50 individuals at the D2 site and 30 individuals at the T1 site. We used estimates of hummock area, perimeter:area, and volume for the comparison. We tested for significant differences in the manual and TopoSeg delineations using a two-tailed *t*-test for unequal variances and a Kolmogorov-Smirnov test. Since the algorithm relies on a single local maximum to delineate individual hummock features, we focused our comparison of site-level hummock size distributions on hummocks with 1 or 2 maxima to ensure the manual delineation and the TopoSeg algorithm identified the same number of features, allowing a more equal comparison.

## 4. Results

### 4.1. Site-level surface model validation

The high-resolution 1 cm microtopographic surface models (Fig. 5) were precise ( $\text{RMSE} = 3.67 \pm 1 \text{ cm}$ ) and accurate ( $\text{bias} = 1.26 \pm 0.1 \text{ cm}$ ) across all sites (Fig. 6, Table 2). The gently sloping lowland sites (L) had substantially higher RMSE and bias than the transition (T) and depression (D) sites. The relatively high error of L-site validation points resulted from either low point density or a complete absence of LiDAR returns (Fig. S4; Supplementary Material). Specifically, we observed overestimation of the surface model when LiDAR was unable to reach the ground surface, leading to the greatest overestimations in sites with dense grass cover (L sites). Overestimation was also common in locations with no LiDAR returns, such as small hollows, where the scanner's oblique view angle was unable to reach. We note that at some sites surface soil moisture may also result in low-intensity returns, but this was not a dominant control on surface model errors. See Fig. S4 for a comparison of validation point error in relation to minimum return intensity.

Lower return density negatively impacted model reconstruction accuracy (Fig. 7, Table 2). In our evaluation of density dependent model error, lower density areas of the models were more positively biased, overestimating the height of the ground surface. Model bias became more positive as density decreased from a saturated point density of 10,000 returns per square meter. Lower point density locations at L sites with dense grasses had higher error, while T and D site models were less affected (Fig. 7; See Fig. S4 in Supplementary Material for LiDAR return density distributions). The density dependent increase in error and bias was apparent across all validation points (Fig. 7A) and across entire sites (Fig. 7B–C). While density affected model error, the relative number of validation points was highly skewed to higher point densities for the D sites, but more evenly distributed for the T and L sites (Supplementary Material; Fig. S5), potentially increasing error

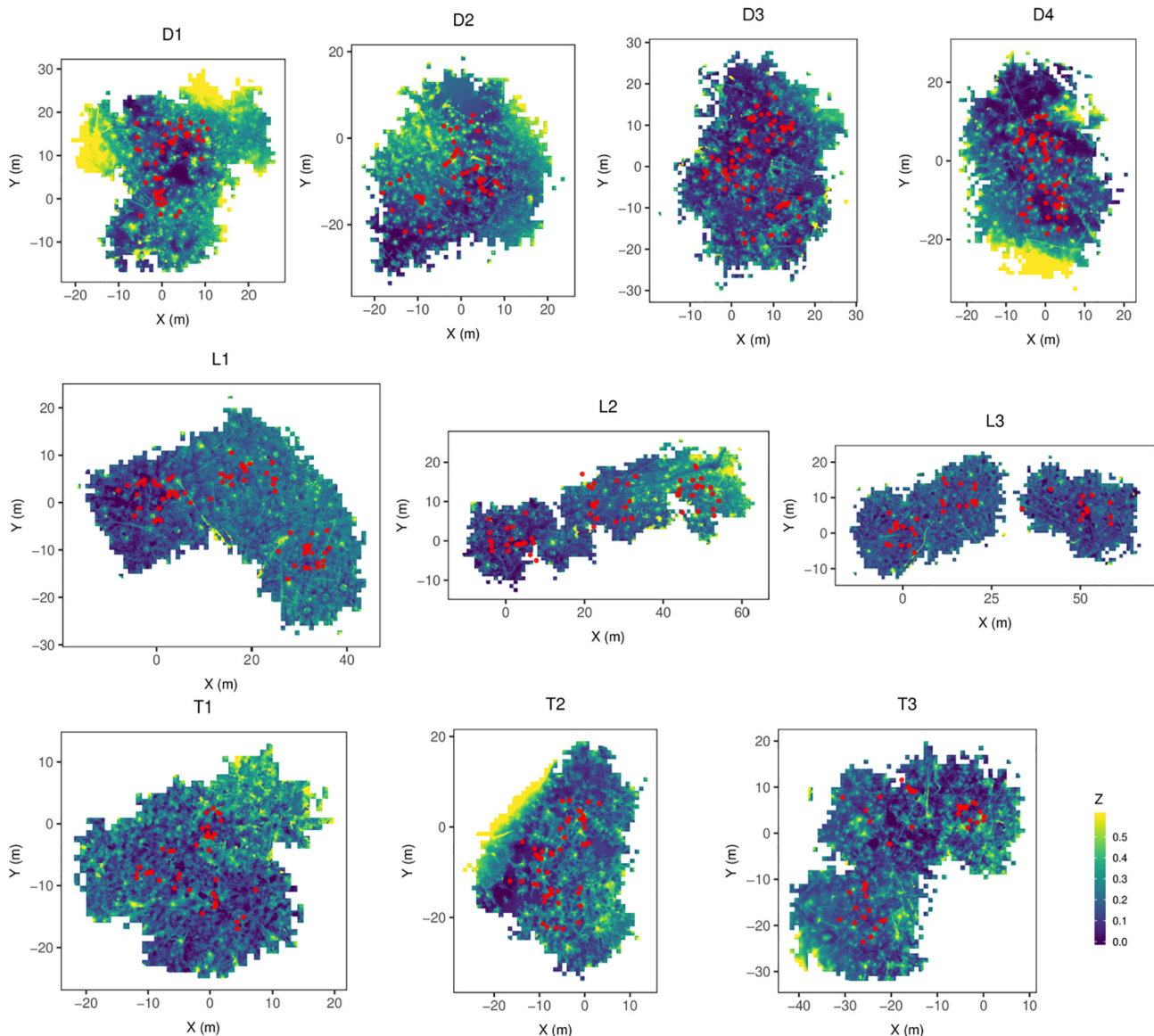


**Fig. 5.** Individual 1 cm site-wide microtopographic surface models produced from Stages 1–3 of the processing pipeline along with validation points used to assess the surface models (red circles). We removed low density areas of the surface models to reduce the impact from uncertain LiDAR returns. Hummocks, hollows, and downed woody debris are clearly visible at D and T sites, while L sites have less evident microtopography. D sites show defined hummock features, while T sites have more complex spatial patterns. L2 shows evidence of impacts from field sampling on the surface model, with low channel-like features where higher compaction occurred from walking through the dense grasses. (For interpretation of the references to color in this figure legend, the reader is referred to the web version of this article.)

estimates due to undersampling in low point density areas.

#### 4.2. Sensitivity analysis of model resolution

Decreasing surface model resolution reduced precision and increased bias of microtopographic surface models (Fig. 8, Table S1). At the highest resolution (1 cm), the T and D sites had error on the order of 2.5–3 cm and had low bias (Fig. 8). Comparatively, at the highest resolution, L sites had higher RMSE (4.7 cm) and positive bias (2.2 cm). Reducing the resolution of the surface reconstruction increased RMSE (Table S1). From 1 to 50 cm resolution, RMSE increased rapidly from 3.4 to 8.4 cm, on average. Above 50 cm, RMSE stabilized between 9 and 11.2 cm. In contrast, bias varied by site (Fig. 8). For example, two L sites were positively biased at higher resolution reconstructions and bias increased as resolution decreased. All other sites had low bias at high model resolution (1–5 cm) but also became positively biased when decreasing resolution from 1 to 20 cm, except D sites, which remained

nearly unbiased at every resolution tested. For all sites, average bias stabilized at around 2 cm at resolutions more coarse than 10 cm (Table S1).

#### 4.3. Sensitivity analysis of hummock classification

Variable selection, model resolution, and classification methodology influenced hummock classification accuracy. Of the five variables tested (Fig. 9) – DEM, roughness, TRI, slope, and LiDAR return intensity – the normalized DEM was the best overall predictor for accurate hummock classification (Fig. 10, Table S2). Depending on model resolution, the DEM contributed between 23 and 62% to overall variable importance, followed by roughness, TRI, and slope (Fig. 9 and Fig. 10). LiDAR return intensity did not improve accuracy at any tested model resolution (Table S2). At the highest resolutions, roughness and TRI are less sensitive to hummock areas (Fig. 10). Of the machine learning approaches, maximum likelihood was the most accurate hummock

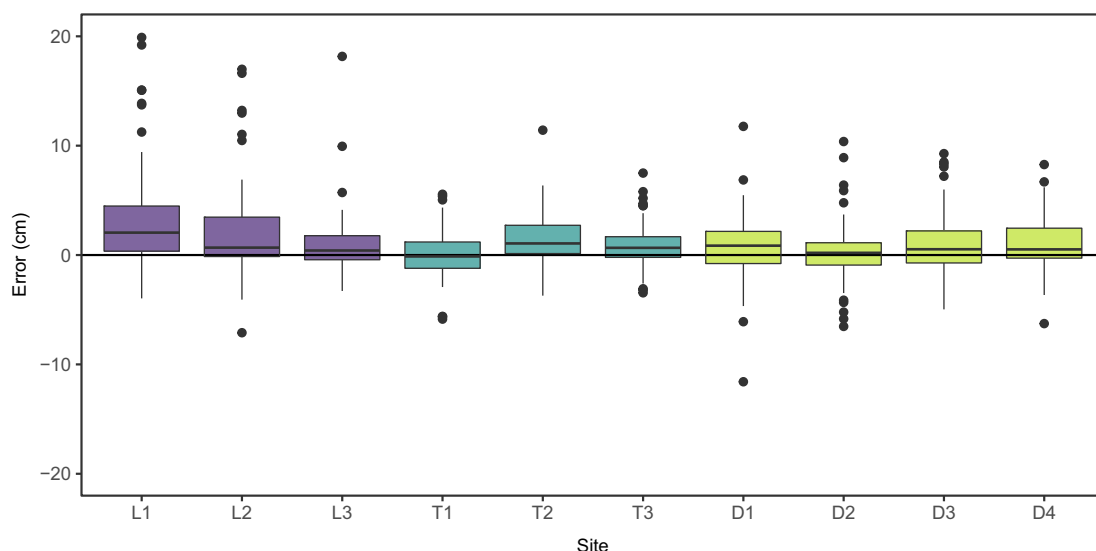


**Fig. 6.** Site-specific distribution of model error at 1 cm resolution. Each data point represents distance from the true surface elevation (solid black line at 0 cm) determined from validation points to the TLS-derived surface model. Sites are colored by their site-type where L are lowland sites, T are transition sites, and D are depression sites. Positive values indicate the surface model overestimated the surface elevation, while negative values are underestimates of surface elevation. Across all sites, the TLS surface models had low error (RMSE = 3.67 cm) and a slight positive bias (1.26 cm).

classification method (70%), while support vector machines were 40% accurate at best (Fig. 11; Fig. 12A). Random forest and k-nearest neighbor performed similarly across the tested resolutions, with k-nearest neighbor performing better at resolutions above 50 cm. The maximum likelihood method at 25 cm resolution was the most accurate machine learning method for distinguishing between hummock and hollow features ( $\text{Kappa} = 0.50$ , Fig. 12B), with decreasing accuracy for more coarse resolution models using all classification methods. The DTA thresholding was 91% accurate for hummock feature classification, but less suitable for differentiating between hummock and hollow areas ( $\text{Kappa} = 0.34$ ).

#### 4.4. Hummock delineation and error assessment

Hummocks delineated from our algorithm were consistent in distribution and dimension with manually delineated hummocks. The algorithm delineation often created multiple hummock features where we manually delineated large, contiguous hummocks, even if multiple local maxima existed. TopoSeg also located hundreds of small ( $< 0.1 \text{ m}^2$ ) hummock features that were not captured with manual delineation, so we limited our statistical analysis to hummocks  $> 0.1 \text{ m}^2$ . Size distributions for both area and volume were statistically indistinguishable for both *t*-test (*p*-value = 0.84 and 0.51, respectively) and Kolmogorov-Smirnov test (*p*-value = 0.40 and 0.88, respectively; Fig. 13). Removing small hummocks resulted in a total loss of 6.58% of hummock area and 3.58% hummock volume from our analysis. We also matched manual- and algorithm-delineated hummock point clouds to pair hummocks from both approaches for a more quantitative error assessment (Fig. 14). Algorithm-delineated hummock area, perimeter:area, and volume estimates had 23%, 19.6%, and 24.1% RMSE, respectively, and the estimates either had low bias or were negatively biased (-9.8%, 0.2%, and -11.9%, respectively).

## 5. Discussion

Fine-scale topographic variation has traditionally been extremely difficult to quantify, but terrestrial LiDAR has enabled automated assessment the microtopography in wetland systems that influences ecological processes. We present an efficient, precise, and accurate method of reconstructing centimeter-scale variation in

microtopography, enabling accurate wetland classification and geometric quantification of individual microtopographic features that holds the potential to standardize wetland microtopographic analysis and thereby improve insights into wetland form and function.

### 5.1. Site-level surface model validation

Site characteristics, such as understory vegetation and inundation, strongly influence model error. Across all site types, the most dominant direct control on surface model error was the LiDAR return density at the ground surface (Fig. 7A). Our analysis of surface density and field observations show the effect of understory vegetation was highest in sites with relatively even cover of grasses, as opposed to sites with clumped, but more dense vegetation, interspersed throughout the site. Other work attempting to capture microtopography with TLS has highlighted return density at the surface and occlusion as a main factor affecting surface reconstruction (Anderson et al., 2010; Barneveld et al., 2013; Baltensweiler et al., 2017; Table 3). In our case, complete occlusion by dense grasses resulted in a positive bias (as much as 20 cm, in some instances) in the surface models, because the initial fine-resolution surface model relies on the lowest possible return in a specific grid cell (Fig. 7C). A potential avenue for improvement of surface models in sites with grasses could be through more extensive or adaptive filtering of spikes and outliers with site-dependent parameters (see Section 3.2.2).

The L sites had the densest and tallest grass coverage and the highest error and bias. In contrast, T sites had less dense grasses, but had a dense understory of other growth forms (e.g., shrubs and saplings). Yet, T sites had comparable error to more open and less occluded sites, suggesting this type of dense understory did not substantially inhibit laser pulses from reaching the underlying surface. We conclude the high-density TLS sampling scheme contributed to the substantially lower than expected model error in the T sites by mitigating the amount of occluded areas. Moreover, the vegetation clumping at T sites, even in the case of dense understory conifers, was less detrimental to model error than the even density of tall grasses at L sites.

The D sites were the least occluded and had minimal error in the surface models, but several were inundated with water, potentially weakening the LiDAR return strength and positively biasing the surface model in hollow depressions. As such, we suggest that future TLS field

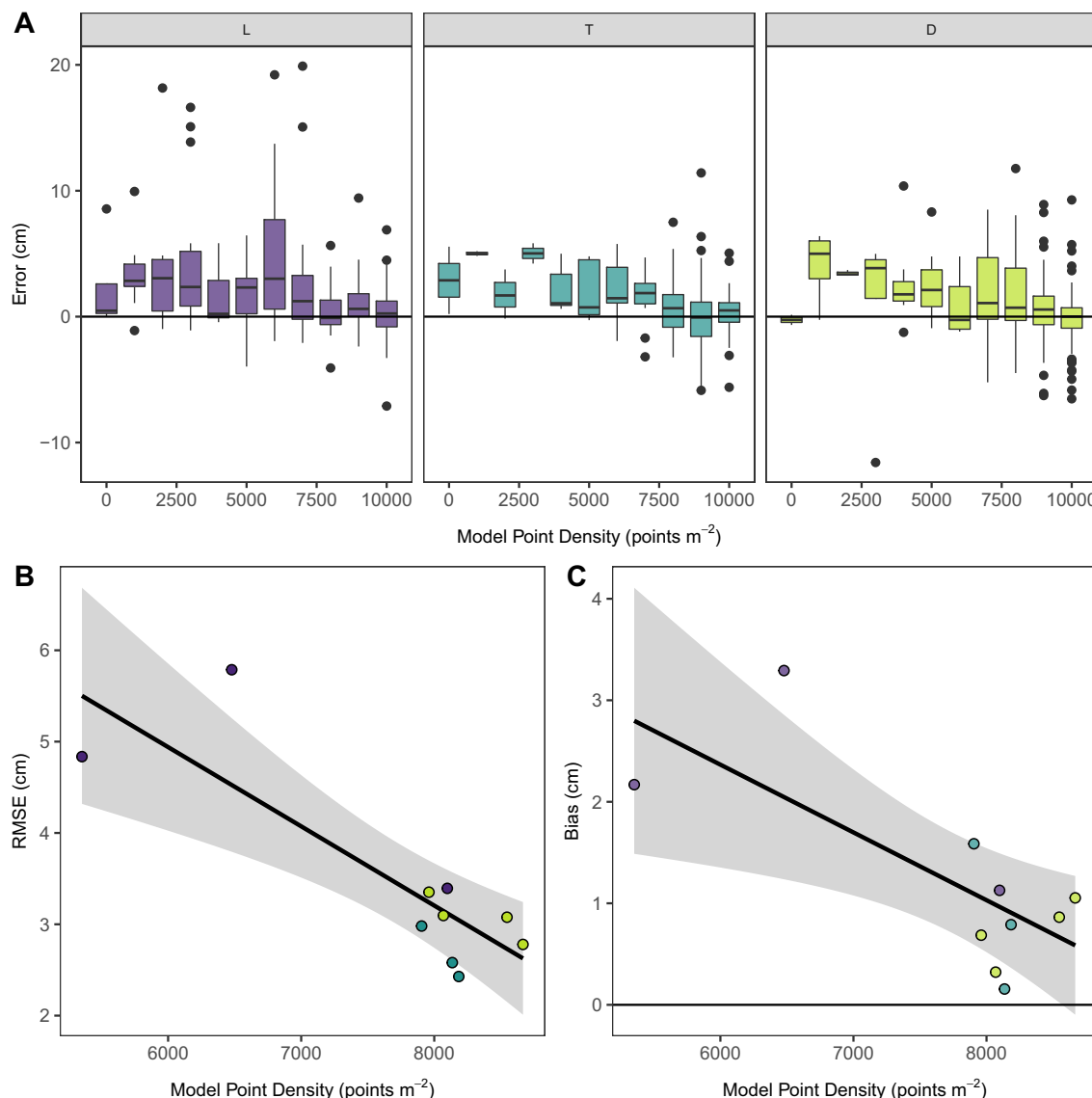


**Fig. 7.** Binned error of the surface model reconstruction at validation points and associated point cloud density for the [A] three site types. [B-C] For all sites, as point cloud density increases, the surface model is more representative of the true topographic surface. In general, [A] areas within a site and  $> 3000 \text{ points } m^{-2}$  and [B-C] sites averaging over  $7500 \text{ points } m^{-2}$  provide the most accurate and precise surface reconstruction across all site types. See Fig. S4 for model point density examples for each site type and Fig. S5 for site type-specific sample distributions referenced in Section 4.1. See Fig. S6 for a comparison of model error for model point density and LiDAR return intensity.

campaigns prioritize dry conditions, or use a TLS unit with a laser wavelength outside of the water absorption range (e.g., 532 nm instead of 905 nm; Milan et al., 2010). Surprisingly, we found no significant relationship between LiDAR return strength and surface model error (Fig. S6, Supplementary Material), suggesting the high-resolution scans may have compensated for a lower number of returns at wet or inundated surfaces. Considering the low error at T sites, the small increase in sampling time with the dense, 10 m gridded scan configuration may be the best approach, even for open understory depression sites. The range of site characteristics in this study spanned near-ideal to less-than-desirable scenarios for TLS application, highlighting the relative stability of TLS-based surface reconstruction and providing clear expectations in surface model reconstruction error moving forward with similar wetland systems.

## 5.2. Sensitivity analysis of model resolution

Fine scale wetland microtopography requires high resolution DEMs

for precise and accurate surface reconstruction. Our sensitivity analysis results suggest surface model resolution strongly controls surface model error, explaining higher errors in previous microtopography studies using more coarse surface models (Table 3). RMSE increased linearly with incremental decreases in resolution from 1 to 50 cm (Fig. 8). The general upward trend of RMSE with decreasing resolution suggests fine-scaled surface variability in hummock and hollow features are unable to be accurately captured without appropriately detailed remote sensing techniques, such as TLS. To a lesser extent, lower resolution models became more positively biased leading to minor model overestimation of the true microtopographic surface. Bias increased until approximately 10–20 cm resolution, above which local microtopographic highs and lows were less accurate. This trend explains the positively biased model surface and the stability in bias and error with lower resolution models. These findings suggest high resolution surface models (1–10 cm) are necessary to accurately capture fine-scale variation in microtopography in many wetland systems. Consequently, we expect that coarse resolution ( $\sim 0.5\text{--}2 \text{ m}$ ) surface models in similar wetlands

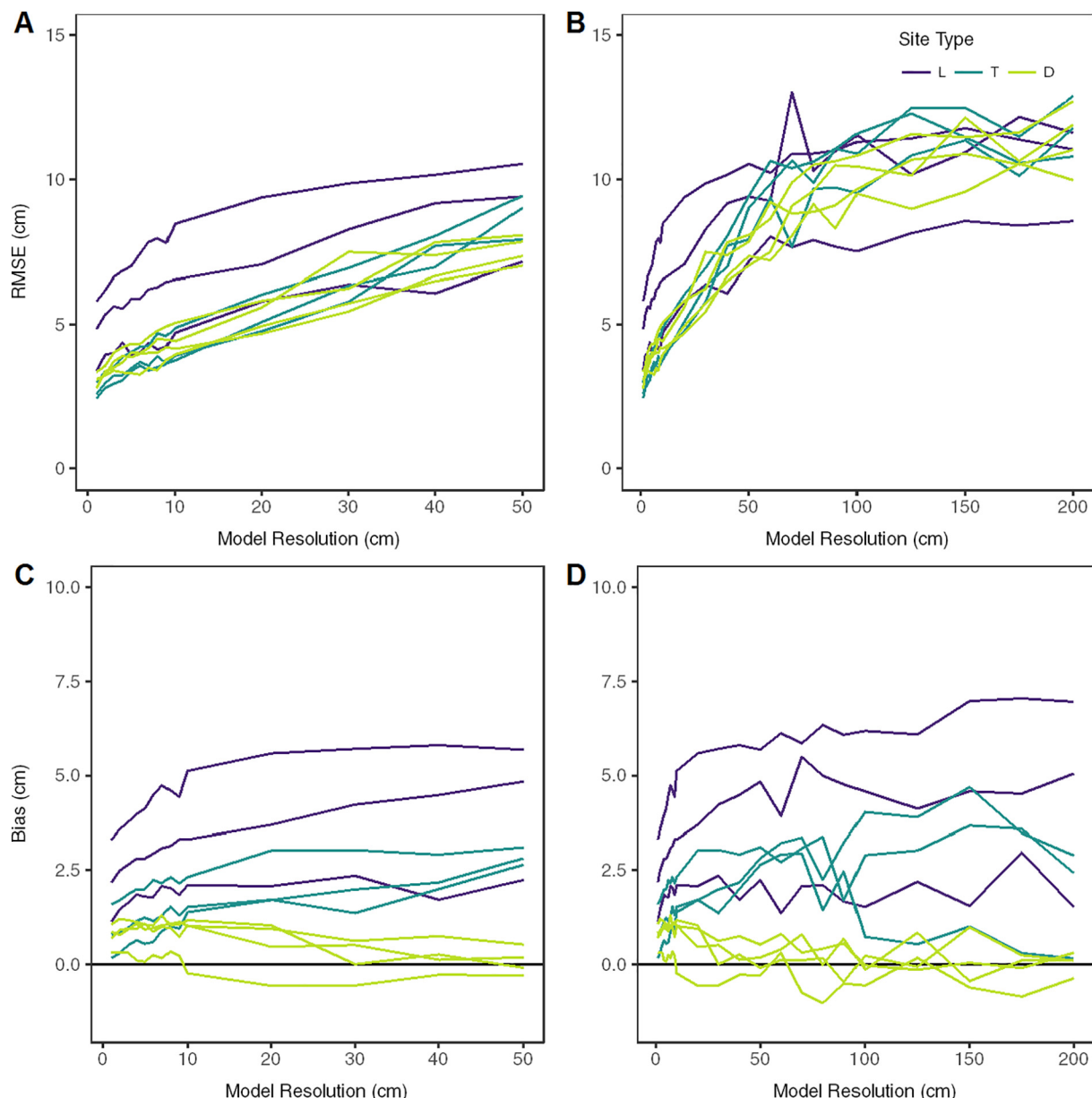


**Fig. 8.** Site-level sensitivity analysis of RMSE and bias with varying model resolution from 1 to 50 cm (top) and 1 to 200 cm (bottom). RMSE and bias increased with coarsening resolution for L and T sites, while D sites remained stable. The L sites had the highest model error, while T and D sites are more precise and accurate. Model error remained stable at approximately 50 cm resolution. See Table S1 for average RMSE and bias under different model resolutions.

derived from airborne LiDAR (Richardson et al., 2010), Unmanned Aerial Vehicle (UAV) LiDAR, or UAV structure from motion (SFM; Mercer and Westbrook, 2016; Kalacska et al., 2017; Lovitt et al., 2017) may be inadequate to capture the vertical and horizontal structure of microtopographic features due to resolution limitations alone (Table 3).

### 5.3. Sensitivity analysis of hummock classification

Accurate classification of microtopographic features is critical for quantifying biogeochemical processes in wetlands. We considered variables typical in landform classification to classify our microtopographic surface models as hummocks or hollows. The DEM, roughness, and TRI were the best microtopographic predictors (Fig. 10). We anticipated LiDAR return intensity would provide additional explanatory power for the classification since hollows tended to be wetter, reducing return intensity at the 905 nm wavelength, but this variable did not add additional explanatory power to the classification (Table S2). The

included variable set showed notable differences between hummock and hollow features, but all products, other than return intensity, were directly derived from the surface model and structural in nature. Additional spectral information could be useful in classifying wetland microtopography. For example, past work has leveraged multispectral datasets with airborne LiDAR to improve wetland classification (Brennan and Webster, 2006; Difebo et al., 2015; Genc et al., 2005; Gilmore et al., 2008; Morris et al., 2005; Rapinel et al., 2015). Spectral data can be added to TLS data, as many commercial instruments include RGB cameras for full color mapping to the point cloud, but the increase in acquisition time and variation in lighting conditions may not justify the small gains in classification accuracy. Applying our methodology to UAV LiDAR datasets may add spectral information that would further improve accuracy.

DEM resolution impacts microtopographic classification accuracy (Fig. 12). For all machine learning classification methods, the most accurate resolution for identifying hummock features was 25 cm.

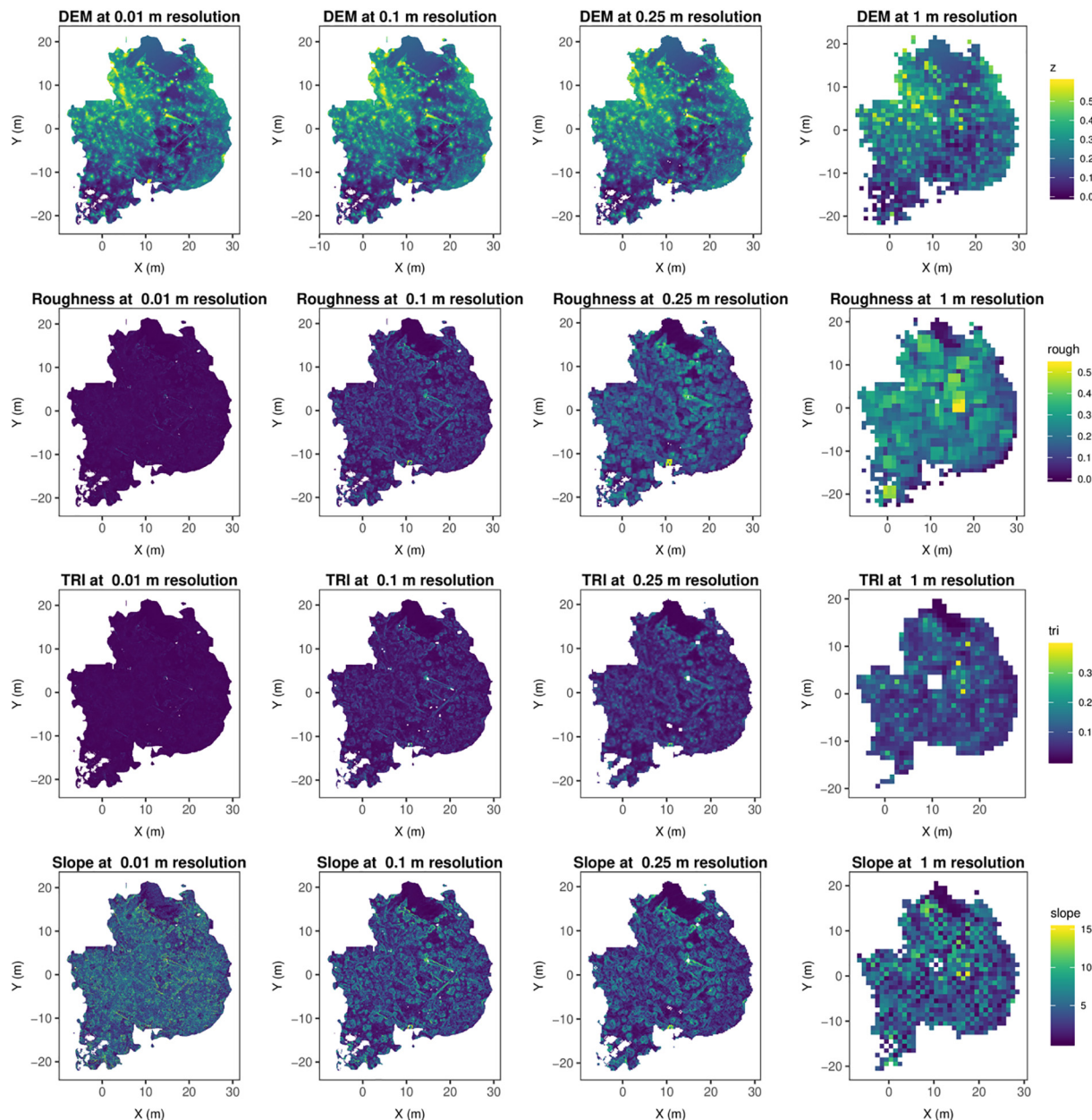


**Fig. 9.** Example surface models and products used to evaluate hummock classification accuracy at site D2 under resolutions ranging from 1 cm to 1 m, from left to right. All products were created directly from a DEM of the same resolution (top row). Roughness, terrain ruggedness index (TRI), and slope effectively highlight hummock features between 10 and 25 cm. LiDAR return intensity (not shown), did not clearly highlight hummock or hollow areas.

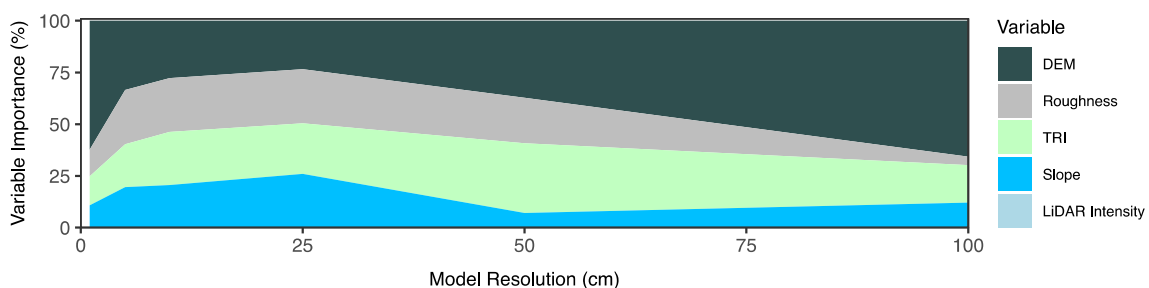
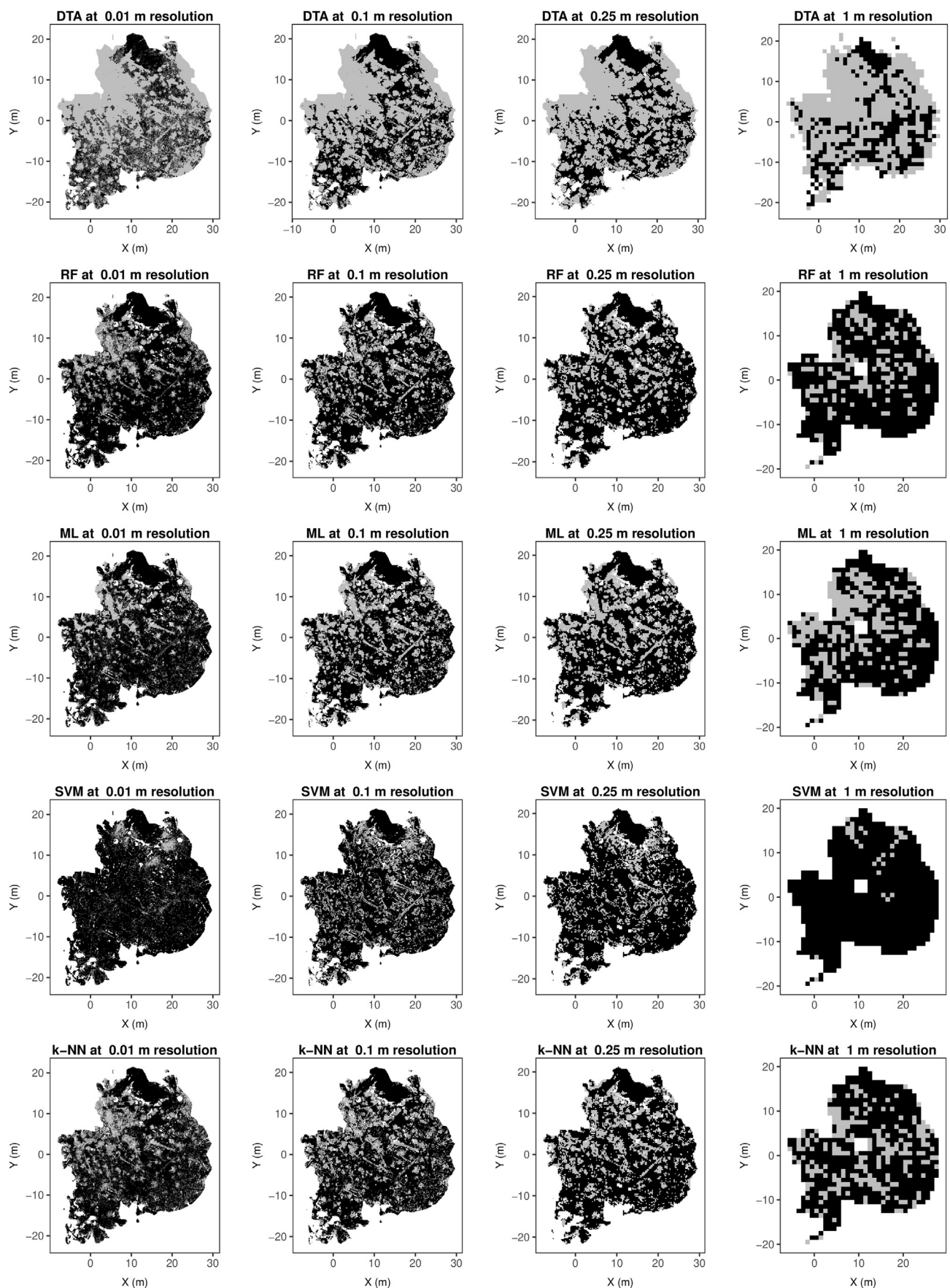


**Fig. 10.** Site-level sensitivity analysis of variable importance using random forest with varying model resolution (1 cm to 1 m) at site D2. At every resolution, the DEM is the best explanatory variable for classifying hummocks and hollows, followed by roughness, terrain ruggedness index (TRI), and slope. LiDAR intensity did not provide any explanatory power for the classification. At coarse resolutions, the DEM and TRI were the best for classifying hummocks and hollows. See Table S2 (Supplementary Material) for absolute and relative variable importance output.



(caption on next page)

**Fig. 11.** Site-level sensitivity analysis of model resolution and five methods of classifying hummock (grey) and hollow (black) features at site D2. We compared DTA thresholding (DTA), random forest (RF), maximum likelihood (ML), support vector machines (SVM), and k-nearest neighbor (k-NN) at model resolutions ranging from 1 cm to 1 m (fine to coarse from left to right). See Fig. S2 for the manually classified hummock and hollow raster used to assess the automatic classification approaches. The DTA approach retained most areas manually classified as hummock (grey), making it ideal for the hummock feature delineation, but underestimated hollow area. Of the machine learning techniques, maximum likelihood classification performed the best at a range of resolutions, with 70% hummock classification accuracy at 25 cm resolution.

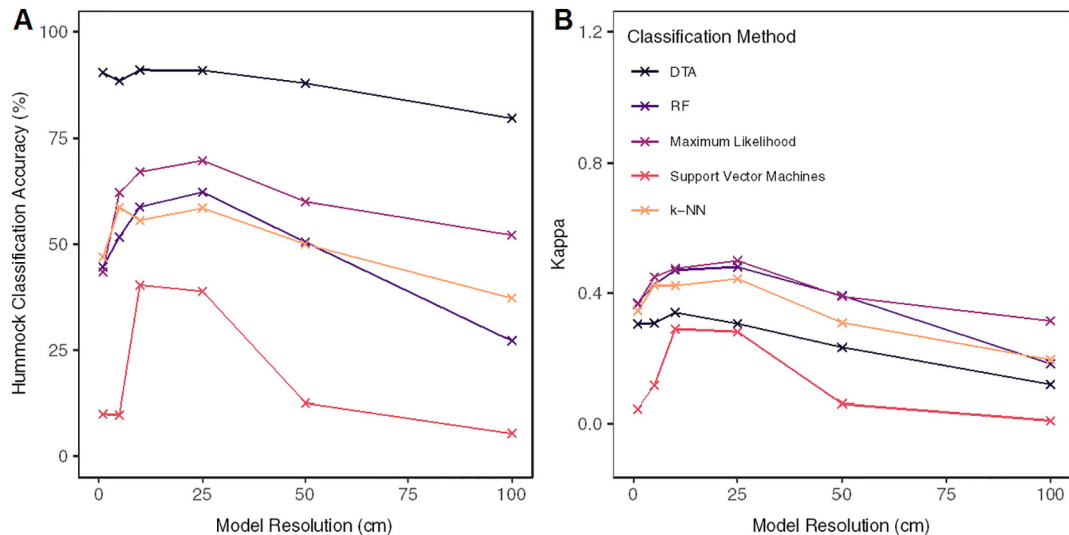


**Fig. 12.** [A] Hummock classification accuracy and [B] Kappa statistic at model resolutions ranging from 1 cm to 1 m, for five hummock classification methods. The DTA threshold classification effectively captured 91% of the hummock area, but underestimated total hollow area (overall accuracy = 65%, Kappa = 0.33). The machine learning classification approaches performed best at 25 cm resolution. For hummock classification, maximum likelihood performed the best (70%), followed by random forest (62%), k-nearest neighbor (59%), and support vector machines (39%). Beyond 25 cm, the accuracy of all machine learning hummock classification methods decreased with decreasing resolution. Overall classification accuracy, distinguishing between hummocks and hollows, was best using maximum likelihood classification at 25 cm resolution (79%). See Table S3 (Supplementary Material) for overall, hummock, and hollow accuracy at the tested resolutions.

Accuracy increased as model resolution decreased across the 1 cm to 25 cm range. Based on visual interpretation of the classification (Fig. 11), we attribute the increase in accuracy to a “smoothing” effect of the surface model from 1 cm to 25 cm, where the topographic products produce more consistent estimates at a given location. For more reliable local estimates of DEM-derived products, smoothing should be considered in surface models finer than 25 cm resolution. A portion of the effect may be scale dependent, so varying the calculation of certain

products like TRI, roughness, and slope to have a fixed window size, independent of model resolution, may improve microtopographic feature classification.

Classification method should be chosen carefully considering the high dependence on surface model resolution. Maximum likelihood classification was consistently the most accurate classification method, performing best at 25 cm resolution. Compared to other methods, maximum likelihood classification accuracy increased dramatically

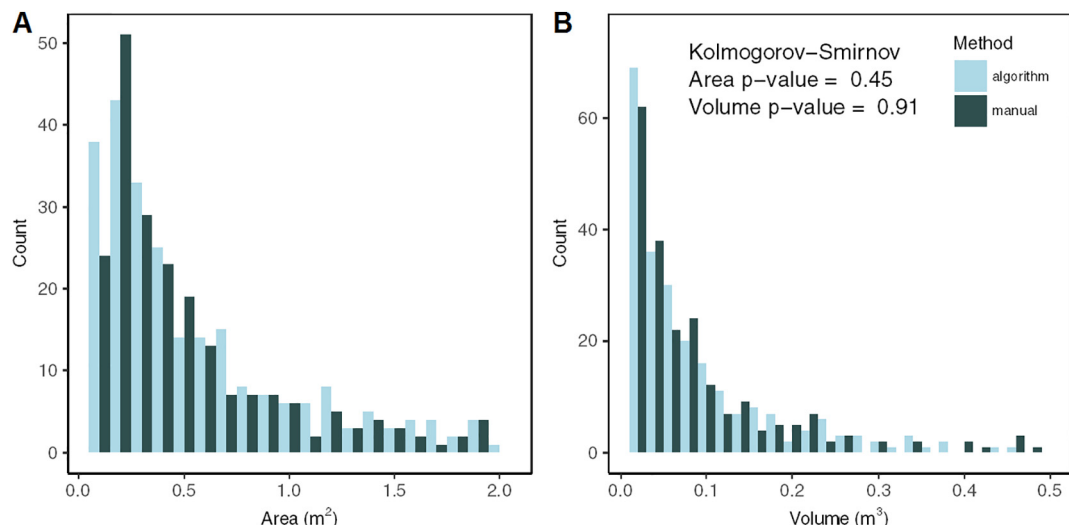


**Fig. 13.** Distribution comparison for manual and algorithm-delineated hummocks. We compared [A] area and [B] volume size distributions and tested for statistical similarity. The algorithm identified a large number of small ( $< 0.1 m^2$ ) hummock features (not shown here) that were not manually delineated, but only accounted for 6.58% of the total hummock area and 3.58% of hummock volume. To compare the distributions equally, we limited the analysis to the range shown above for the Kolmogorov Smirnov test (p-values shown).

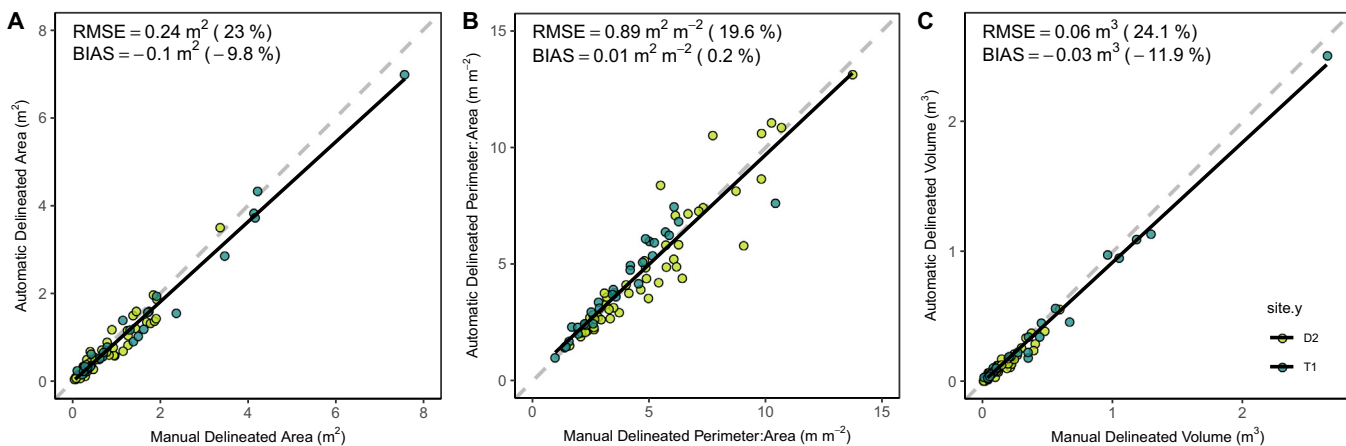


**Fig. 14.** Assessment of hummock delineation method for retrieving feature-level [A] area, [B] perimeter:area ratio, and [C] volume estimates. Points are colored according to sites with differing levels of hummock complexity. The depression site (D2; light green) had smaller hummocks with low edge complexity while the transition site (T1; blue) had larger, more complex hummock shapes. The dashed grey line represents the 1:1 line. See Fig. S6 for a visual comparison of the manual and automatically detected hummock features. (For interpretation of the references to color in this figure legend, the reader is referred to the web version of this article.)

from 43% to 70% from 1 cm to 25 cm resolution (Fig. 11). In contrast, support vector machines (SVD) should be avoided for high-resolution classification of microtopography based on poor performance in this analysis. Upon visual inspection of the SVD method classification, we found the method was most sensitive to steep sloped areas, on the outer edge of hummocks, but otherwise inaccurate. K-nearest neighbor classification accuracy followed a similar pattern, albeit slightly lower, as random forest and maximum likelihood. While we limited our analysis of classification method accuracy to those commonly used with landform classification, other methods may be promising under certain conditions.

#### 5.4. Hummock delineation and error assessment

Hummock- and hollow-scale feature delineation provides new and relevant information on microtopographic structures in wetlands. To our knowledge, no previous work has attempted to delineate microtopographic features using terrestrial LiDAR. TopoSeg – our novel

adaptation of an airborne LiDAR forestry tool typically used for tree segmentation – allows for hummock and hollow classification and segmentation that was previously prohibitively time consuming and qualitative (Nungesser, 2003; Lorente et al., 2012). Factors that control the size, shape, and distribution of wetland hummocks remain an open question (Larsen and Harvey, 2010; Heffernan et al., 2013) with important global modeling (Shi et al., 2015) and restoration (US Environmental Protection Agency, 2015; Creed et al., 2017) ramifications, but this work presents a first attempt to rapidly quantify these features using an objective standardized methodology.

Manual hummock classification is inherently subjective due to edge complexity, posing a major challenge for efficient manual assessment of precision and accuracy of the TopoSeg method. For instance, Lovitt et al. (2014) reported the majority of hummock misclassification occurred at the boundary of hummock and hollow areas, calling into question the very definition of the hummock edge. For this reason, we compared hummock level statistics such as total area, length-area ratio, and volume at two sites, where manual delineation was feasible and our

**Table 3**

Comparison of resolution and validation error from past studies quantifying high-resolution wetland topography. See Supplementary Material for more details on each validation method.

Technique	Device	Location	Resolution (m)	Extent	Elevation error statistics		Reference
					(ha)	RMSE (m)	
TLS	Faro Focus 120 3D	Swamps, Minnesota	0.01	0.09	0.0367	0.0126	This study
	Leica HDS 3000	Ombrotrophic bog, UK	0.1	0.0079	0.108–0.175		Anderson et al., 2010
	Faro Focus 120 3D	Forest, Switzerland	0.2	2	0.12	-0.05	Baltensweiler et al., 2017
ALS	Leica ScanStation2	Semiarid hillslope, Spain			0.001–0.002		Rodríguez-Caballero et al., 2016
	Riegl VZ-1000 m	Forest, Switzerland	0.2	2	0.15	-0.1	Baltensweiler et al., 2017
	Optech ALTM 2050	Mangroves, Australia	0.3	92	0.042		Knight et al., 2009
SFM	Leica ALS70	Upland plains, Canada	0.3	24,000	0.14–0.16		Hopkinson et al., 2005
	Leica ALS50	Peatland, UK	0.5	0.01	0.029	0.0004	Luscombe et al. 2015
	Optech ALTM 3100	Floodplains, Poland	0.5	7300	0.4	0.13	Miroslaw et al. 2016
Others	Leica ALS70	Treed bog, Canada	0.76	61	0.84	0.47	Lovitt et al., 2017
	Leica ALS50	Mangroves, Australia	1	20	0.061	0.036	Griffin et al., 2010
	Optech ALTM 3100	Floodplains, Australia	1	5500	0.02–0.03	0.08–0.11	Rayburg et al., 2009
	Leica ALS70	Peatlands, Canada	1	31–1500	0.14 ± 0.07		Langlois et al., 2017
Others	Leica ALS70	Peatlands, Upper Midwest USA	1.8	1330–1840	0.0988		Richardson et al., 2010
	Canon 550D digital SLR camera	Mossy area, East Antarctica	0.02	2	0.044	0.005	Lucieer et al., 2014
	Panasonic Lumix DMC-GH2	Paleontological site, western Turkey	0.042	5.5	0.159		Roosevelt, 2014
	Canon PowerShot D10	Alpine peatland, Canada	0.39		0.044–0.138	0.23–0.54	Mercer and Westbrook, 2016
Others	Aeryon Scout	Treed bog, Alberta Canada	0.59	61	0.13–0.40	-0.1–0.23	Lovitt et al., 2017

confidence was higher. Delineation error stayed relatively constant throughout the hummock size range, suggesting site-level estimates are likely unbiased and our method is suitable for upscaling. As such, this validation approach could be adaptable in similar systems such as bogs, with larger and more easily identifiable features. Notably, superior small hummock identification compared to manual observation is evident in the present algorithm given the large number of small hummocks ( $< 0.1 \text{ m}^2$ ) delineated at each site. While small hummocks may only modestly increase total site-level hummock area and volume, large numbers of small hummocks can dramatically increase site-level perimeter:area, disproportionately increasing the number of sharp redox gradients and biogeochemical hot spots (cf. Cohen et al. 2016). Our method overcomes some of the issues with hummock size definition, since it is automatic and of extremely high resolution, requiring no additional effort to capture small scale features. Nonetheless, we expect further developments and refinements to the TopoSeg algorithm that will allow for rapid quantitative assessment of hummock and hollows, effectively reducing reliance on manual methods and ambiguous microtopographic definitions.

### 5.5. Future work: upscaling and applications

The high-resolution approach highlighted in this work for quantifying wetland microtopography represents an important step to bridge current gaps in measurement scales. TLS captures a scale of topographic variation that can be linked to a suite of wetland biogeochemical processes (e.g., nutrient and carbon cycling; Baltensweiler et al., 2017; Lovitt et al., 2014; Cheng and Basu, 2017) and habitat conditions (e.g., Malhotra et al., 2016; Čelik and Vreš, 2018). As such, high-resolution microtopographic models will facilitate upscaling to more extensive remote sensing approaches, allowing ecosystem-scale elemental storage and flux estimates that integrate dynamic and heterogeneous surface processes. Improved resolution from future UAV LiDAR, or structure from motion in low density vegetation, may enable upscaling by covering larger spatial extents, while providing high-resolution data for microtopographic surface reconstruction and delineation described here. Moreover, the TopoSeg algorithm can easily be applied to equivalent high-resolution 3D data acquired with UAV LiDAR in similar wetland systems (Lovitt et al., 2017; Lovitt et al., 2014). Moving forward, a focus on upscaling will be the most important next step in tying microtopographic processes to complex ecosystem modeling efforts (Miao et al., 2017).

The algorithms in this study enable larger landscape-scale high-resolution microtopographic surface reconstruction in wetland systems that will be critical in better estimating fine-scale variation in wetland processes that influence broader landscape-scale phenomena. Wetlands have the highest density of soil carbon globally while disproportionately holding the largest fraction of global soil carbon (20–30%; Lal, 2008). The spatial distribution of these soil carbon stocks and associated emissions within and across systems is directly influenced by microtopography (Page et al., 2007; Sundari et al., 2012), through modulation of soil saturation and associated decomposition rates (Holden, 2005; Strack et al., 2006). High spatial variability in soil carbon pools and the simplification of soil profiles as planar surfaces across broad scales (Kimble et al., 2002) makes landscape-scale soil carbon estimates uncertain (Mitsch et al., 2013), likely resulting in a systematic underestimation of carbon stored in wetlands. Accurate estimates of current wetland carbon stores are crucially important given their role in global budgets and their vulnerability to climate change via enhanced decomposition rates (Macreadie et al., 2013). By leveraging the algorithms described in this study to accurately resolve, or even predict, microtopographic distributions in wetlands over large spatial extents we anticipate considerable improvements in landscape or even global biogeochemical models (Shi et al., 2015; Lehmann and Rillig, 2014).

## 6. Conclusion

Traditional approaches of quantifying wetland microtopography lack detail and spatial continuity, limiting inference of wetland patterns and processes. In the current study, we developed and assessed a method of high-resolution microtopographic surface reconstruction, classification, and feature delineation using terrestrial laser scanning that covers entire 0.09 ha portions of wetlands. Our results indicate high-resolution surface models, on the order of 1–10 cm, are necessary to precisely capture vertical and horizontal microtopographic structure, with model error increasing with decreasing DEM resolution, losing sensitivity to microtopography above 50 cm. Hummock and hollow features are most accurately classified at 25 cm resolution using maximum likelihood, but DTA threshold classification effectively retains hummock areas for individual feature delineation. Our novel feature delineation algorithm – TopoSeg – was precise and accurate, enabling more consistent future microtopography characterization across a range of remote sensing platforms. Our approach is currently the most precise method of quantifying microtopography in wetland systems using terrestrial laser scanning and can be adapted for broad applicability to similar systems globally.

## Acknowledgments

We would like to thank our funding sources: Minnesota Forest Resources Council and Virginia Tech Institute for Critical Technology and Applied Science Fellowship. Also, thank you to the three anonymous reviewers of this manuscript and the *Remote Sensing of Environment* editorial team.

## Appendix A. Supplementary data

Supplementary data to this article can be found online at <https://doi.org/10.1016/j.rse.2019.111271>.

## References

- Acreman, M., Holden, J., 2013. How wetlands affect floods. *Wetlands* 33 (5), 773–786. <https://doi.org/10.1007/s13157-013-0473-2>.
- Anderson, C.J., Lockaby, B.G., 2007. Soils and biogeochemistry of tidal freshwater forested wetlands. In: Conner, W.H., Doyle, T.W., Krauss, K.W. (Eds.), *Ecology of Tidal Freshwater Forested Wetlands of the Southeastern United States*. Springer, New York, NY.
- Anderson, K., Bennie, J., Wetherelt, A., 2010. Laser scanning of fine scale pattern along a hydrological gradient in a peatland ecosystem. *Landscape Ecol.* 25, 477–492. <https://doi.org/10.1007/s10980-009-9408-y>.
- Atkins, J.W., Bohrer, G., Fahey, R.T., Hardiman, B.S., Morin, T.H., Stovall, A.E.L., Zimmerman, N., Gough, C.M., 2018. Quantifying vegetation and canopy structural complexity from terrestrial LiDAR data using the forestr package. *Methods Ecol. Evol.* <https://doi.org/10.1111/2041-210X.13061>.
- Baltensweiler, A., Walther, L., Ginzler, C., Suttor, F., Purves, R.S., Hanewinkel, M., 2017. Terrestrial laser scanning improves digital elevation models and topsoil pH modelling in regions with complex topography and dense vegetation. *Environ. Model Softw.* 95, 13–21. <https://doi.org/10.1016/j.envsoft.2017.05.009>.
- Barneveld, R.J., Seeger, M., Maalen-Johansen, I., 2013. Assessment of Terrestrial Laser Scanning Technology for Obtaining High-Resolution DEMs of Soils: TLS FOR HIGH-RESOLUTION DEMS. *Earth Surf. Process. Landf.* 38 (1), 90–94. <https://doi.org/10.1002/esp.3344>.
- Brennan, R., Webster, T.L., 2006. Object-oriented land cover classification of lidar-derived surfaces. *Can. J. Remote. Sens.* 32, 162–172. <https://doi.org/10.5589/m06-015>.
- Bubier, J.L., Moore, T.R., Bellisario, L., Comer, N.T., Crill, P.M., 1995. Ecological controls on methane emissions from a northern Peatland complex in the zone of discontinuous permafrost, Manitoba, Canada. *Glob. Biogeochem. Cycles* 9, 455–470. <https://doi.org/10.1029/95GB02379>.
- Capps, K.A., Rancatti, R., Tomczyk, N., Parr, T.B., Calhoun, A.J., Hunter, M., 2014. Biogeochemical hotspots in forested landscapes: the role of vernal pools in denitrification and organic matter processing. *Ecosystems* 17 (8), 1455–1468. <https://doi.org/10.1007/s10021-014-9807-z>.
- Casey, S.T., Cohen, M.J., Acharya, S., Kaplan, D.A., Jawitz, J.W., 2016. Hydrologic controls on aperiodic spatial organization of the ridge-slough patterned landscape. *Hydrolog. Earth Syst. Sci.* 20 (11), 4457–4467.
- Čelik, T., Vreš, B., 2018. Microtopography determines the habitat quality of a threatened peatland butterfly at its southern range margin. *J. Insect Conserv.* 1–14.

- Cheng, F.Y., Basu, N.B., 2017. Biogeochemical hotspots: role of small water bodies in landscape nutrient processing. *Water Resour. Res.* 53 (6), 5038–5056.
- CloudCompare (version 2.10.1) [GPL software], 2018. Retrieved from. <http://www.cloudcompare.org/>.
- Cohen, M.J., Creed, I.F., Alexander, L., Basu, N.B., Calhoun, A.J.K., Craft, C., D'Amico, E., et al., 2016. Do geographically isolated wetlands influence landscape functions?". *Proc. Natl. Acad. Sci.* 113 (8), 1978–1986. <https://doi.org/10.1073/pnas.1512650113>.
- Courtwright, J., Findlay, S.E.G., 2011. Effects of microtopography on hydrology, physicochemistry, and vegetation in a tidal swamp of the Hudson River. *Wetlands* 31, 239–249. <https://doi.org/10.1007/s13157-011-0156-9>.
- Creed, I.F., Lane, C.R., Serran, J.N., Alexander, L.C., Basu, N.B., Calhoun, A.J., DeKeyser, E., 2017. Enhancing protection for vulnerable waters. *Nat. Geosci.* 10 (11), 809.
- Difebo, A., Richardson, M., Price, J., 2015. Fusion of Multispectral Imagery and LiDAR Digital Terrain Derivatives for Ecosystem Mapping and Morphological Characterization of a Northern Peatland Complex. vols. 399–412<https://doi.org/10.1201/b18210-22>.
- Ehrenfeld, J.G., 1995. Microsite differences in surface substrate characteristics in Chamaecyparis swamps of the New Jersey pinelands. *Wetlands* 15, 183–189. <https://doi.org/10.1007/BF03160672>.
- Frei, S., Fleckenstein, J.H., 2014. Representing effects of micro-topography on runoff generation and sub-surface flow patterns by using superficial rill/depression storage height variations. *Environ. Model Softw.* 52, 5–18.
- Frei, S., Peiffer, S., 2016. Exposure times rather than residence times control redox transformation efficiencies in riparian wetlands. *J. Hydrol.* 543, 182–196.
- Genc, L., DEWITT, B., Smith, S., 2005. Determination of wetland vegetation height with LiDAR. *Turk. J. Agric. For.* 28.
- Gilmore, M.S., Wilson, E.H., Barrett, N., Civco, D.L., Prisloe, S., Hurd, J.D., Chadwick, C., 2008. Integrating multi-temporal spectral and structural information to map wetland vegetation in a lower Connecticut River tidal marsh. *Remote Sens. Environ.* 112, 4048–4060. <https://doi.org/10.1016/j.rse.2008.05.020>.
- Griffin, L.F., Knight, J.M., Dale, P.E.R., 2010. Identifying mosquito habitat microtopography in an Australian mangrove forest using LiDAR derived elevation data. *Wetlands* 30, 929–937. <https://doi.org/10.1007/s13157-010-0089-8>.
- Heffernan, J.B., Watts, D.L., Cohen, M.J., 2013. Discharge competence and pattern formation in peatlands: a meta-ecosystem model of the Everglades ridge-slough landscape. *PLoS One* 8, e64174.
- Hohenthal, J., Alho, P., Hyypäät, J., Hyypäät, H., 2011. Laser scanning applications in fluvial studies. *Prog. Phys. Geogr.* 35, 782–809. <https://doi.org/10.1177/0309133111414605>.
- Holden, J., 2005. Peatland hydrology and carbon release: why small-scale process matters. *Philos. Trans. R. Soc. A Math. Phys. Eng. Sci.* 363, 2891–2913. <https://doi.org/10.1098/rsta.2005.1671>.
- Hopkinson, C., Chasmer, L.E., Sass, G., Creed, I.F., Sitar, M., Kalbfleisch, W., Treitz, P., 2005. Vegetation class dependent errors in lidar ground elevation and canopy height estimates in a boreal wetland environment. *Can. J. Remote. Sens.* 31, 191–206. <https://doi.org/10.5589/m05-007>.
- Kalacska, M., Chmura, G.L., Lucas, O., Bérubé, D., Arroyo-Mora, J.P., 2017. Structure from motion will revolutionize analyses of tidal wetland landscapes. *Remote Sens. Environ.* 199, 14–24. <https://doi.org/10.1016/j.rse.2017.06.023>.
- Kimble, J.M., Lal, R., Birdsey, R., Heath, L.S., 2002. *The Potential of U.S. Forest Soils to Sequester Carbon and Mitigate the Greenhouse Effect*. CRC Press.
- Knight, J.M., Dale, P.E.R., Spencer, J., Griffin, L., 2009. Exploring LiDAR data for mapping the micro-topography and tidal hydro-dynamics of mangrove systems: an example from Southeast Queensland, Australia. *Estuar. Coast. Shelf Sci.* 85, 593–600. <https://doi.org/10.1016/j.ecss.2009.10.002>.
- Korpela, I., Koskinen, M., Vasander, H., Holopainen, M., Minkkinen, K., 2009. Airborne Small-Footprint Discrete-Return LiDAR Data in the Assessment of Boreal Mire Surface Patterns, Vegetation, and Habitats (For. Ecol. Manage.). 258 (7), 1549–1566.
- Lal, R., 2008. Carbon sequestration. *Philos. Trans. R. Soc., B* 363, 815–830. <https://doi.org/10.1098/rstb.2007.2185>.
- Langlois, M.N., Richardson, M.C., Price, J.S., 2017. Delineation of peatland lagg boundaries from airborne LiDAR. *J. Geophys. Res. Biogeosci.* 122, 2191–2205. <https://doi.org/10.1002/2017JG003835>.
- Larsen, L.G., Harvey, J.W., 2010. How vegetation and sediment transport feedbacks drive landscape change in the Everglades and wetlands worldwide. *Am. Nat.* 176, E66–E79.
- Lehmann, J., Rillig, M., 2014. Distinguishing variability from uncertainty. *Nat. Clim. Chang.* 4, 153. <https://doi.org/10.1038/nclimate2133>.
- Liang, X., Kankare, V., Hyypäät, J., Wang, Y., Kukko, A., Haggrén, H., Yu, X., Kaartinen, H., Jaakkola, A., Guan, F., Holopainen, M., Vastaranta, M., 2016. Terrestrial laser scanning in forest inventories. *ISPRS J. Photogramm. Remote Sens.* <https://doi.org/10.1016/j.isprsjprs.2016.01.006>.
- Lorente, M., Parsons, W.F.J., Périé, C., Munson, A.D., 2012. Spectral analysis discerns pattern and feedback in natural- and anthropogenic-disturbed boreal black spruce forests. *Oikos* 121, 772–782. <https://doi.org/10.1111/j.1600-0706.2011.19777.x>.
- Lovitt, J., Rahman, M.M., McDermid, G.J., 2017. Assessing the value of UAV photogrammetry for characterizing terrain in complex Peatlands. *Remote Sens.* 9. <https://doi.org/10.3390/rs9070715>.
- Lovitt, J., Rahman, M.M., Saraswati, S., McDermid, G.J., Strack, M., Xu, B., 2014. UAV remote sensing can reveal the effects of low-impact seismic lines on surface morphology, hydrology, and methane (CH<sub>4</sub>) release in a boreal treed bog. *J. Geophys. Res. Biogeosci.* 123, 1117–1129. <https://doi.org/10.1002/2017JG004232>.
- Macreadie, P.I., Hughes, A.R., Kimbro, D.L., 2013. Loss of 'blue carbon' from coastal salt marshes following habitat disturbance. *PLoS One* 8, e69244. <https://doi.org/10.1371/journal.pone.0069244>.
- Malhotra, A., Roulet, N.T., Wilson, P., Giroux-Bougard, X., Harris, L.I., 2016. Ecohydrological feedbacks in peatlands: an empirical test of the relationship among vegetation, microtopography and water table. *Ecohydrology* 9 (7), 1346–1357.
- Mercer, J.J., Westbrook, C.J., 2016. Ultrahigh-resolution mapping of peatland microform using ground-based structure from motion with multiview stereo. *J. Geophys. Res. Biogeosci.* 121, 2901–2916. <https://doi.org/10.1002/2016JG003478>.
- Miao, G., Noormets, A., Domec, J.C., Fuentes, M., Trettin, C.C., Sun, G., McNulty, S.G., King, J.S., 2017. Hydrology and microtopography control carbon dynamics in wetlands: implications for partitioning ecosystem respiration in a coastal plain forested wetland. *Agric. For. Meteorol.* 247, 343–355.
- Milan, D.J., Heritage, G.L., Large, A.R.G., Entwistle, N.S., 2010. Mapping hydraulic biotopes using terrestrial laser scan data of water surface properties. *Earth Surf. Process. Landf.* 35, 918–931. <https://doi.org/10.1002/esp.1948>.
- Miroslaw-Swiatek, D., Szporak-Wasilewska, S., Michałowski, R., Kardel, I., Grygoruk, M., 2016. Developing an algorithm for enhancement of a digital terrain model for a densely vegetated floodplain wetland. *J. Appl. Remote. Sens.* 10. <https://doi.org/10.1117/1.JRS.10.036013>.
- Mitsch, W.J., Bernal, B., Nahlik, A.M., Mander, Ü., Zhang, L., Anderson, C.J., Jørgensen, S.E., Brix, H., 2013. Wetlands, carbon, and climate change. *Landscape Ecol.* 28, 583–597. <https://doi.org/10.1007/s10980-012-9758-8>.
- Khosravipour, A., Skidmore, A.K., Isenburg, M., Wang, T., Hussin, Y.A., 2014. Generating pit-free canopy height models from airborne lidar. *Photogramm. Eng. Remote Sens.* 80 (9), 863–872. <https://doi.org/10.14358/PERS.80.9.863>.
- Morris, J.T., Porter, D., Neet, M., Noble, P.A., Schmidt, L., Lapine, L.A., Jensen, J.R., 2005. Integrating LiDAR elevation data, multi-spectral imagery and neural network modelling for marsh characterization. *Int. J. Remote Sens.* 26, 5221–5234. <https://doi.org/10.1080/01431160500219018>.
- Moser, K., Ahn, C., Noe, G., 2007. Characterization of microtopography and its influence on vegetation patterns in created wetlands. *Wetlands* 27, 1081–1097. [https://doi.org/10.10672/0277-5212\(2007\)27\[1081,COMAI\]2.0.CO;2](https://doi.org/10.10672/0277-5212(2007)27[1081,COMAI]2.0.CO;2).
- Nungesser, M.K., 2003. Modelling microtopography in boreal peatlands: hummocks and hollows. *Ecol. Model.* 165, 175–207. [https://doi.org/10.1016/S0304-3800\(03\)00067-X](https://doi.org/10.1016/S0304-3800(03)00067-X).
- Othmani, A., Piboule, A., Krebs, M., Stolz, C., Voon, L.L.Y., 2011. Towards automated and operational forest inventories with T-Lidar. In: 11th International Conference on LiDAR Applications for Assessing Forest Ecosystems (Silvi Laser 2011).
- Page, S.E., Banks, C.J., Rieley, J.O., 2007. Tropical peatlands: distribution, extent and carbon storage-uncertainties and knowledge gaps. *Peatlands International* 2 (2), 26–27.
- Pau, G., Fuchs, F., Sklyar, O., Boutros, M., Huber, W., 2010. EBImage—an R package for image processing with applications to cellular phenotypes. *Bioinformatics* 26, 979–981. <https://doi.org/10.1093/bioinformatics/btq046>.
- Peterson, J.E., Baldwin, A.H., 2004. Variation in wetland seed banks across a tidal freshwater landscape. *Am. J. Bot.* 91, 1251–1259.
- Pouliot, R., Rochefort, L., Karofeld, E., Mercier, C., 2011. Initiation of Sphagnum moss hummocks in bogs and the presence of vascular plants: is there a link? *Acta Oecol.* 37, 346–354. <https://doi.org/10.1016/j.actao.2011.04.001>.
- R Core Team, 2017. R: A Language and Environment for Statistical Computing. R Foundation for Statistical Computing, Vienna, Austria. <http://www.R-project.org/>.
- Rapinel, S., Hubert-Moy, L., Clément, B., 2015. Combined use of LiDAR data and multi-spectral surface observation imagery for wetland habitat mapping. *Int. J. Appl. Earth Obs. Geoinf.* 37, 56–64. <https://doi.org/10.1016/j.jag.2014.09.002>.
- Rayburg, S., Thoms, M., Neave, M., 2009. A comparison of digital elevation models generated from different data sources. *Geomorphology* 106, 261–270. <https://doi.org/10.1016/j.geomorph.2008.11.007>.
- Richardson, M., Millard, K., 2018. Chapter 15: Geomorphic and Biophysical Characterization of Wetland Ecosystems with Airborne LiDAR: Concepts, Methods, and a Case Study. *High Spatial Resolution Remote Sensing: Data, Analysis, and Applications*. Boca Raton. <https://www.taylorfrancis.com/books/9780429893001>.
- Richardson, M.C., Fortin, M.-J., Branfireun, B.A., 2009. Hydrogeomorphic edge detection and delineation of landscape functional units from lidar digital elevation models: hydrogeomorphic edge detection with lidar. *Water Resour. Res.* 45 (10). <https://doi.org/10.1029/2008WR007518>.
- Richardson, M.C., Mitchell, C.P.J., Branfireun, B.A., Kolka, R.K., 2010. Analysis of airborne LiDAR surveys to quantify the characteristic morphologies of northern forested wetlands. *J. Geophys. Res. Biogeosci.* 115. <https://doi.org/10.1029/2009JG000972>.
- Rodríguez-Caballero, E., Afana, A., Chamizo, S., Solé-Benet, A., Canton, Y., 2016. A new adaptive method to filter terrestrial laser scanner point clouds using morphological filters and spectral information to conserve surface micro-topography. *ISPRS J. Photogramm. Remote Sens.* 117, 141–148. <https://doi.org/10.1016/j.isprsjprs.2016.04.004>.
- Roosevelt, C.H., 2014. Mapping site-level microtopography with Real-Time Kinematic Global Navigation Satellite Systems (RTK GNSS) and Unmanned Aerial Vehicle Photogrammetry (UAVP). *Open Archaeology* 1 (1). <https://doi.org/10.2478/opar-2014-0003>.
- Roussel, J.-R., Auty, D., 2018. lidR: Airborne LiDAR Data Manipulation and Visualization for Forestry Applications.
- Rusu, R.B., Cousins, S., 2011. 3D Is Here: Point Cloud Library (PCL). In: IEEE International Conference on Robotics and Automation (ICRA), (Shanghai, China). SCENE (version 5.4.4.41689), 2015. FARO Technologies Inc.
- Semlitsch, R.D., Bodie, J.R., 2003. Biological criteria for buffer zones around wetlands and riparian habitats for amphibians and reptiles. *Conserv. Biol.* 17 (5), 1219–1228. [www.jstor.org/stable/3588947](https://www.jstor.org/stable/3588947).
- Sheffer, E., von Hardenberg, J., Yizhaq, H., Shachak, M., Meron, E., 2013. Emerged or imposed: a theory on the role of physical templates and self-organisation for vegetation patchiness. *Ecol. Lett.* 16 (2), 127–139.

- Shi, X., Thornton, P.E., Ricciuto, D.M., Hanson, P.J., Mao, J., Sebestyen, S.D., Griffiths, N.A., Bisht, G., 2015. Representing northern peatland microtopography and hydrology within the community land model. *Biogeosciences* 12, 6463–6477. <https://doi.org/10.5194/bg-12-6463-2015>.
- Stenberg, L., Tuukkanen, T., Finér, L., Marttila, H., Piirainen, S., Kløve, B., Koivusalo, H., 2016. Evaluation of erosion and surface roughness in peatland forest ditches using pin meter measurements and terrestrial laser scanning: evaluation of erosion and surface roughness in peatland forest ditches. *Earth Surf. Process. Landf.* 41, 1299–1311. <https://doi.org/10.1002/esp.3897>.
- Stovall, A.E.L., Shugart, H.H., 2018. Improved biomass calibration and validation with terrestrial LiDAR: implications for future LiDAR and SAR missions. *IEEE J. Sel. Top. Appl. Earth Observations Rem. Sens.* PP 1–11. <https://doi.org/10.1109/JSTARS.2018.2803110>.
- Stovall, A.E.L., Vorster, A.G., Anderson, R.S., Evangelista, P.H., Shugart, H.H., 2017. Non-destructive aboveground biomass estimation of coniferous trees using terrestrial LiDAR. *Remote Sens. Environ.* 200, 31–42. <https://doi.org/10.1016/j.rse.2017.08.013>.
- Stovall, A.E.L., Anderson-Teixeira, K.J., Shugart, H.H., 2018. Assessing terrestrial laser scanning for developing non-destructive biomass allometry. *For. Ecol. Manag.* 427, 217–229. <https://doi.org/10.1016/j.foreco.2018.06.004>.
- Strack, M., Waddington, J.M., Rochefort, L., Tuittila, E.-S., 2006. Response of vegetation and net ecosystem carbon dioxide exchange at different peatland microforms following water table drawdown: WATER TABLE AND PEATLAND CO<sub>2</sub> EXCHANGE. *J. Geophys. Res. Biogeosci.* 111<https://doi.org/10.1029/2005JG000145>. n/a-n/a.
- Stribling, J., Glahn, O., Chen, X., Cornwell, J., 2006. Microtopographic variability in plant distribution and biogeochemistry in a brackish-marsh system. *Mar. Ecol. Prog. Ser.* 320, 121–129. <https://doi.org/10.3354/meps320121>.
- Sullivan, P.F., Arens, S.J., Chimner, R.A., Welker, J.M., 2008. Temperature and microtopography interact to control carbon cycling in a high arctic fen. *Ecosystems* 11 (1), 61–76. <https://doi.org/10.1007/s10021-007-9107-y>.
- Sundari, S., Hirano, T., Yamada, H., Kusin, K., Limin, S., 2012. Effect of groundwater level on soil respiration in tropical peat swamp forests. *Agric. Meteorol.* 68 (2), 121–134. <https://doi.org/10.2480/agrmet.68.2.6>.
- US Environmental Protection Agency, 2015. *Connectivity of Streams and Wetlands to Downstream Waters: A Review and Synthesis of the Scientific Evidence*. EPA/600/R-14/475F. US Environmental Protection Agency Washington, DC.
- Watts, D.L., Cohen, M.J., Heffernan, J.B., Osborne, T.Z., 2010. Hydrologic modification and the loss of self-organized patterning in the ridge-slough mosaic of the Everglades. *Ecosystems* 13, 813–827. <https://doi.org/10.1007/s10021-010-9356-z>.